OAW
Austrian Academy
of Sciences

JKU
JOHANNES KEPLER
UNIVERSITY LINZ

Adaptive Strategies for High Order FEM in Elastoplasticity

Peter G. Gruber

Adaptive Strategies for High Order FEM in Elastoplasticity

Peter G. Gruber[*]

March 18, 2010

Abstract

This work is concerned with the numerical solution of variational problems in elastoplasticity. Since the whole class of all possible elastoplastic problems is too large for a common treatment, we restrict ourselves to the investigation of problems which are quasi-static, and where strain and displacement are related linearly. Further, the homogeneous and isotropic material should obey the Prandtl-Reuß flow and a linear hardening principle. After an implicit Euler discretization in time, it is possible to derive a one-time step minimization problem, which can be solved by a Newton-like method.

Each iteration step represents a linear boundary value problem, which has to be discretized in space and approximately solved on the computer. Due to regularity reasons, the application of a Finite Element Method (FEM) of low and high order (*hp*-FEM) looks promising. Roughly speaking, low order FEM is used in regions of the domain where the solution is expected to have low regularity (plastic zones), while the use of high order FEM speeds up the convergence of the approximate solution in regions where the solution has high regularity (elastic zones).

We discuss a several different *hp*-adaptive Strategies, particularly a technique is applied, where the regularity of the solution is estimated by analyzing the expansion of the Finite Element solution with respect to an L_2-orthogonal polynomial basis. Also the application of a Boundary Concentrated FEM to elastoplastic problems is discussed and numerically tested.

1 Introduction

In this article we discuss the application of High Order Finite Element Methods (hp-FEM) to elastoplastic problems with linear hardening. We consider elastoplastic problems, modelled by a quasi-static balance equation, a linearized strain field, homogeneous and isotropic constitutive laws, and the Prandtl-Reuß flow rule. Moreover, we assume elastoplasticity with linear isotropic hardening. Several computation techniques for solving the elastoplastic problem with other kinds of hardening can be found in [37, 13, 46, 4, 35, 34], whereas problems without hardening, i. e. perfect Prandtl Reuß plasticity, are discussed in [48, 49, 47].

By multiplying the balance equation and the flow rule with test functions and integrating over the domain, a time-dependent variational inequality is obtained. The unique solvability of this inequality in proper Sobolev spaces was shown in [31] utilizing results for general variation inequalities [22]. After an implicit Euler time discretization we end up with one variational inequality per time step.

Such variational inequality can be equivalently formulated [25] as a minimization problem with respect to the displacement and the stress fields, called the elastoplastic one time step minimization problem in *dual formulation*,

$$J(u, \sigma) \to \min .$$

After discretizing in space, the problem can be solved on the computer by the return mapping algorithm [46], which is well-known in the field of elastoplasticity. Another option is to formulate the variational inequality as a minimization problem with respect to the displacement and the plastic strain fields, called the elastoplastic one time step minimization problem in *primal formulation* [15],

$$J(u, p) \to \min .$$

Numerical algorithms to solve such a problem are discussed, e. g., in [14, 4].

Utilizing the primal formulation, the problem can be reformulated as a minimization problem

$$J(u) \to \min ,$$

with a functional J depending only on the displacement field [26]. The corresponding minimization functional is strictly convex and continuously Fréchet differentiable with an explicitly known derivative $D\,J$. Finding the solution to the elastoplastic problem means, to find the displacement field, for which the derivative of the functional vanishes, i. e.

$$D\,J(u) = 0 .$$

Since the functional J is not quadratic, i. e., the derivative DJ is non-linear, the problem has to be solved iteratively. A steepest descent method could be applied, but this method converges only linearly, and we can do better. As discussed in [26], a slant Newton method can be applied, which, after a spatial Finite Element Galerkin discretization, converges super-linearly to the discrete solution. The chosen spatial discretization results in one linear system per slant Newton step, which has to be solved on the computer. At this point the question arises, which spatial discretization should be chosen.

In [10, 36] it is shown, that the solution to the elastoplastic problem with linear hardening is twice weakly differentiable everywhere apart from the boundary, and even analytic in open balls of the domain, where the plastic strain vanishes. This motivates the use of hp-FEM for elastoplastic problems with linear hardening. The term hp-FEM stands for the mixed use of low order Finite Element Methods (h-FEM) and high order Finite Element Methods (p-FEM). In h-FEM the accuracy of the approximate solution is increased by decreasing the mesh size h, while the polynomial degree p of the shape functions is kept constant. Conversely, in p-FEM the mesh size is constant, and the polynomial degree p of the shape functions is increased in order to obtain a better approximation. The combination of both is called hp-FEM. One chooses adaptively for each element, whether to refine it in h-FEM manner, or to increase the polynomial degree of the local shape functions in p-FEM manner.

For certain problems (apart from elastoplasticity), a proper adaptive strategy in hp-FEM leads to exponential convergence [5] of the Finite Element solution, versus the polynomial convergence in h- and p-FEM. The key idea is to locally apply h-FEM where the solution has low regularity, and to use p-FEM where the solution is smooth.

Some adaptive strategies for hp-FEM applied to the Poisson problem are discussed in [23], under the assumption, that the mesh consists of only triangles (in 2D) or tetrahedrons (in 3D). For the 2D case, we transfer these results and strategies from scalar to vector valued boundary value problems, such as we have to solve at every slant Newton step of the elastoplastic solver, as presented in Section 2. Moreover, the application of a Zone Concentrated Finite Element Method (ZC-FEM), closely related to the Boundary Concentrated Finite Element Method (BC-FEM) [33], to elastoplasticity is also discussed in this work. Finally, numerical examples show the success of the several adaptive strategies.

2 Mathematical Modeling

The mathematical modeling of elastoplastic problems has a long history, and many approaches have been proposed in order to model how materials react under the influence of inner and outer forces. A wide overview on this topic is given in the monographs [27, 46, 2]. We will briefly introduce one of many possible classical formulations, and then turn to the weak formulation and time discretization. On basis of the so called primal weak formulation, we will derive a minimization problem regarding the displacement, which can be solved by a Newton-like method.

2.1 Classical Formulation

Let $\Theta := (0, T)$ be a time interval, and let Ω be a bounded Lipschitz domain in the space $\mathbb{R}^3$. The equilibrium of forces in the quasi-static case reads

$$-\operatorname{div}(\sigma(x,t)) = f(x,t) \quad \text{for } (x,t) \in \Omega \times \Theta, \tag{1}$$

where $\sigma(x,t) \in \mathbb{R}^{3\times3}$ is called *Cauchy's stress tensor* and $f(x,t) \in \mathbb{R}^3$ is called the *volume force* acting at the material point $x \in \Omega$ at the time $t \in \Theta$. Let $u(x,t) \in \mathbb{R}^3$ be the *displacement* of the body, and let

$$\varepsilon(u) := \frac{1}{2}\left(\nabla u + (\nabla u)^T\right) \tag{2}$$

denote the linearized *Green-St. Venant strain tensor*. The strain ε is split additively into an elastic part e and a plastic part p, that is,

$$\varepsilon = e + p. \tag{3}$$

The stress-strain relation is given by Hook's law

$$\sigma = \mathbb{C}e, \tag{4}$$

where the fourth-order *elasticity tensor* $\mathbb{C} \in \mathbb{R}^{3\times3\times3\times3}$ is defined by $\mathbb{C}_{ijkl} := \lambda\delta_{ij}\delta_{kl} + \mu(\delta_{ik}\delta_{jl} + \delta_{il}\delta_{jk})$. Here, $\lambda > 0$ and $\mu > 0$ denote the *Lamé* constants, and δ_{ij} is the *Kronecker-symbol*.

Let the boundary $\Gamma := \partial\Omega$ be split into a *Dirichlet-part* Γ_D and a *Neumann-part* Γ_N, which satisfy $\Gamma_D \cup \Gamma_N = \Gamma$ and $\Gamma_D \cap \Gamma_N = \emptyset$. We assume the boundary conditions

$$u = u_D \quad \text{on } \Gamma_D, \tag{5}$$

$$\sigma n = g \quad \text{on } \Gamma_N, \tag{6}$$

4

where $n(x, t)$ is the exterior unit normal, $u_D(x, t) \in \mathbb{R}^3$ denotes a prescribed displacement and $g(x, t) \in \mathbb{R}^3$ is a prescribed traction. By neglecting the plastic strain term in (3), i.e. $p = 0$, the system (1) - (6) describes a purely elastic behavior of the continuum Ω.

Another two properties incorporating the admissibility of a stress field σ with respect to a certain *hardening law* and the time evolution of the plastic strain p are required. Therefore, we introduce the *hardening parameter* α and call a tuple (σ, α) the *generalized stress*. Such generalized stress is called *admissible*, if for a given convex *yield functional* ϕ there holds

$$\phi(\sigma, \alpha) \leq 0 \,. \tag{7}$$

The explicit form of ϕ depends on the choice of the *hardening law*. In this paper we concentrate on the *isotropic* hardening law, where the hardening parameter α is a scalar function $\alpha : \Omega \to \mathbb{R}$ and the yield functional ϕ is then defined by

$$\phi(\sigma, \alpha) := \begin{cases} \|\mathrm{dev}\,\sigma\|_F - \sigma_y(1 + H\alpha) & \text{if } \alpha \geq 0, \\ +\infty & \text{if } \alpha < 0. \end{cases} \tag{8}$$

Here, the *Frobenius norm* $\|A\|_F := \langle A,\, A\rangle_F^{1/2}$ is defined via the scalar product $\langle A,\, B\rangle_F := \sum_{ij} a_{ij} b_{ij}$ for $A = (a_{ij}) \in \mathbb{R}^{3 \times 3}$ and $B = (b_{ij}) \in \mathbb{R}^{3 \times 3}$ and the *deviator* is defined for square matrices as $\mathrm{dev}\,A = A - \frac{\mathrm{tr}\,A}{\mathrm{tr}\,I}I$, where the *trace* of a matrix is defined by $\mathrm{tr}\,A = \langle A,\, I\rangle_F$ with I denoting the identity matrix. The material constants σ_y and H are both positive real numbers and called *yield stress* and *modulus of hardening*, respectively. The second plastic property addresses the time development of the *generalized plastic strain* $(p, -\alpha)$, which we assume to satisfy *Prandtl-Reuß' normality law*

$$\langle (\dot{p}, -\dot{\alpha})\,, \,(\tau, \beta) - (\sigma, \alpha)\rangle_F \leq 0 \qquad \forall (\tau, \beta) \text{ satisfying } \phi(\tau, \beta) \leq 0 \,, \tag{9}$$

where $\dot{p}$ and $\dot{\alpha}$ denote the first time derivatives of p and α. The initial conditions read

$$p(x, 0) = p_0(x) \quad \text{and} \quad \alpha(x, 0) = \alpha_0(x) \quad \forall x \in \Omega \,, \tag{10}$$

with given initial values $p_0 : \Omega \to \mathbb{R}_{\mathrm{sym}}^{3 \times 3}$ and $\alpha_0 : \Omega \to [0, \infty[$.

Problem 1. Find (u, p, α) such, that (1)–(7), (9) and (10) are satisfied.

Note, that Problem 1 is a simplified description of the elastoplastic deformation of a body. First, the second time derivative of the displacement u is ignored in the balance of momentum (1). Thus, only problems with

slowly varying velocity fields, so called quasi-static problems, are modelled correctly. Second, the relation between strain and displacement in (2) is just a first order approximation of the true relation

$$\varepsilon(u) = \frac{1}{2} \left(\nabla u + \nabla u^T + \nabla u^T \nabla u \right) .$$

Third, the constitutive laws, such as Hooke's law (4), the flow law (9) and the hardening law (7) and (8), describe only a very specific behaviour of the material. Let be mentioned, that an eminently general mathematical formulation of elasto- and viscoplastic deformation problems is outlined and discussed in great detail in the monograph [2].

Here, we solely study the numerical solution to Problem 1. However, an extension to other elastoplastic problems is possible and promising.

2.2   Weak Formulation

In this subsection we derive a weak formulation out of Problem 1. Hence the well known Sobolev and Lebesgue spaces have to be defined: Let $V := [H^1(\Omega)]^3$, and $Q := [L_2(\Omega)]^{3\times3}_{\text{sym}}$. The associated scalar products and norms are

$$\langle u, v \rangle_V := \int_\Omega \left(\langle u, v \rangle_F + \langle \nabla u, \nabla v \rangle_F \right) \, \mathrm{d}x , \qquad \|v\|_V := \langle v, v \rangle_V^{1/2} ,$$

$$\langle p, q \rangle_Q := \int_\Omega \langle p, q \rangle_F \, \mathrm{d}x , \qquad\qquad\qquad \|q\|_Q := \langle q, q \rangle_Q^{1/2} .$$

Let be mentioned, that a time-dependent variational inequality can be obtained by the multiplication of (1) and (9) with test functions, integration, partial integration and subsequent adding of both (see [27] for details). It is known [31], that this time-dependent variational inequality has a unique solution $u \in \{v \in H^1(\Theta; V) \mid v_{|\Gamma_D} = u_D\}$, $p \in H^1(\Theta; Q)$, and $\alpha \in H^1(\Theta; L_2(\Omega))$.

However, the numerical treatment requires a time discretization of the a time-dependent variational inequality. Therefore, let $N_\Theta \in \mathbb{N}$, $\tau := T/N_\Theta$ and $\Theta_\tau := \{t_k := k\tau \mid k \in \{0, \dots, N_\Theta\}\}$ be a discretization of the time interval $\Theta = [0, T]$. We introduce the notation

$$u_k := u(t_k), \;\; p_k := p(t_k), \;\; \alpha_k := \alpha(t_k), \;\; f_k := f(t_k), \;\; g_k := g(t_k), \;\; \dots ,$$

and approximate time derivatives by the backward difference quotients, i. e.,

$$\dot{p}_k \approx (p_k - p_{k-1})/\tau \quad \text{and} \quad \dot{\alpha}_k \approx (\alpha_k - \alpha_{k-1})/\tau.$$

Consequently, the time dependent variational inequality simplifies to a sequence of time independent variational inequalities of the second kind [27], each of which can be equivalently expressed by a minimization problem. Let $\overline{\mathbb{R}} = \mathbb{R} \cup \{\pm\infty\}$ be the set of extended real numbers, and the functional $\bar{J}_k : V \times Q \to \overline{\mathbb{R}}$ defined as

$$J_k(v, q) = \frac{1}{2}\|\varepsilon(v) - q\|_{\mathbb{C}}^2 + \psi_k(q) + l_k(v) \,, \tag{11}$$

with

$$\langle q_1 \,, q_2 \rangle_{\mathbb{C}} \;:=\; \int_{\Omega} \langle \mathbb{C}\, q_1(x) \,, q_2(x) \rangle_F \,\mathrm{d}x \,, \qquad \|q\|_{\mathbb{C}} \;:=\; \langle q \,, q \rangle_{\mathbb{C}}^{1/2} \,, \tag{12}$$

$$\psi_k(q) \;:=\; \begin{cases} \int_{\Omega} \left(\frac{1}{2}\tilde{\alpha}_k(q)^2 + \sigma_y\|q - p_{k-1}\|_F\right) \,\mathrm{d}x & \text{if } \operatorname{tr} q = \operatorname{tr} p_{k-1} \,, \\ +\infty & \text{else} \,, \end{cases} \tag{13}$$

$$l_k(v) \;:=\; \int_{\Omega} f_k \cdot v \,\mathrm{d}x + \int_{\Gamma_N} g_k \cdot v \,\mathrm{d}s \,, \tag{14}$$

$$\tilde{\alpha}_k(q) \;:=\; \alpha_{k-1} + \sigma_y H\|q - p_{k-1}\|_F \,. \tag{15}$$

The resulting one time step minimization problem reads [14]:

Problem 2. Let $k \in \{1, \ldots, N_\Theta\}$ denote a given time step, $f_k \in H^{-1}(\Omega)$, $g_k \in H^{-1/2}(\Gamma_N)$, $p_{k-1} \in Q$ and $\alpha_{k-1} \in L_2(\Omega)$ be given such, that $\alpha_{k-1} \geq 0$ almost everywhere. Find $(u_k, p_k) \in V_D \times Q$ such that

$$\bar{J}_k(u_k, p_k) \leq \bar{J}_k(v, q) \,,$$

with $\bar{J}_k$ defined in (11), holds for all $(v, q) \in V_D \times Q$.

The convex functional $\bar{J}_k$ expresses the mechanical energy of the deformed system at the $k-$th time step. The goal is to find a displacement u_k and a plastic strain p_k such that the energy $\bar{J}_k$ is minimized. The unique solvability of Problem 2 can be shown with classical convex analysis results [24]. The hardening parameter $\alpha_k \in L_2(\Omega)$ does not appear in Problem 2 directly, but can be calculated analytically in dependence on the plastic strain by $\alpha_k = \tilde{\alpha}_k(p_k)$ defined as in equation (15). Various strategies have been introduced to solve the minimization in Problem 2. C. Carstensen investigated a separated minimization in the displacement v and in the plastic strain q alternately and proved the linear convergence of the resulting method in [14].

2.3 Minimization with Respect to Displacements

Another interesting technique is to reduce Problem 2 to a minimization problem with respect to the displacements v only [26]. Due to a theorem of

J. J. Moreau [40] the functional $J_k : V \to \mathbb{R}$ with $J_k(v) := \inf_{q \in Q} \bar{J}_k(v, q)$ is well defined, strictly convex, and Fréchet differentiable. There exists a unique minimizer with respect to the plastic strain field $\tilde{p}_k : Q \to Q$, such that $\bar{J}_k(v, \tilde{p}_k(\varepsilon(v))) = J_k(v)$ holds for all v in V. The explicit form of p_k was calculated for the first time in [4] and reads

$$\tilde{p}_k(\varepsilon(v)) = \frac{1}{2\mu + \sigma_y^2 H^2} \max\{0, \phi_{k-1}(\tilde{\sigma}_k(\varepsilon(v)))\} \frac{\operatorname{dev} \tilde{\sigma}_k(\varepsilon(v))}{\|\operatorname{dev} \tilde{\sigma}_k(\varepsilon(v))\|_F} + p_{k-1}, \quad (16)$$

where

$$\tilde{\sigma}_k(q) := \mathbb{C}(q - p_{k-1}) \quad \text{and} \quad \phi_{k-1}(\sigma) := \|\operatorname{dev} \sigma\|_F - \sigma_y(1 + H\,\alpha_{k-1}). \quad (17)$$

As already mentioned, the functional J_k is Fréchet differentiable. The differential reads

$$D\,J_k(v\,;\,w) = \langle \varepsilon(v) - \tilde{p}_k(\varepsilon(v))\,,\,\varepsilon(w) \rangle_\mathbb{C} - l_k(w) \quad \forall w \in V \qquad (18)$$

with the scalar product $\langle \circ\,,\,\diamond \rangle_\mathbb{C}$ defined in (12) and l_k defined in (14).

With these considerations, we are able to reformulate Problem 2 by

Problem 3. Let $k \in \{1, \ldots, N_\Theta\}$ denote a given time step, $f_k \in H^{-1}(\Omega)$, $g_k \in H^{-1/2}(\Gamma_N)$, $p_{k-1} \in Q$ and $\alpha_{k-1} \in L_2(\Omega)$ be given such, that $\alpha_{k-1} \geq 0$ almost everywhere. Find $u_k \in V_D$ such that for all $v \in V_D$ there holds

$$J_k(u_k) \leq J_k(v)\,,$$

where the functional $J_k : V \to \mathbb{R}$ is defined

$$J_k(v) = \frac{1}{2}\|\varepsilon(v) - \tilde{p}_k(\varepsilon(v))\|_\mathbb{C}^2 + \psi_k(\tilde{p}_k(\varepsilon(v))) + l_k(v)\,, \qquad (19)$$

with ε, ψ_k, l_k, and $\tilde{p}_k$ defined in (2), (13), (14), and (16).

Remark 1. Functional J_k is Fréchet differentiable, with $D\,J_k(v\,;\,w)$ as in (18).

Remark 2. The plastic strain $p_k \in Q$ and hardening parameter $\alpha_k \in L_2(\Omega)$ do not appear in Problem 3 directly, but can be calculated analytically in dependence on the displacement by $p_k = \tilde{p}_k(\varepsilon(u_k))$ defined in (16), and $\alpha_k = \tilde{\alpha}_k(p_k)$ defined in (15).

Remark 3. Note, that since the problem can be shown to be uniquely solvable [26], it is sufficient to find the displacement $u_k \in V_D$, such that for all test functions $w \in V_0$ there holds

$$D\,J_k(u_k\,;\,w) = 0\,. \qquad (20)$$

8

The minimizer $\tilde{p}_k$ in (16) is a continuous mapping of Q into Q. Thus, $D\,J_k(v\,;w)$ in (18) is continuous with respect to v as well, and a gradient method could be used for a numerical solution. A higher order optimization method, such as the Newton method, requires the second derivative of J_k, which, due to the term $\max\{0,\cdot\}$ in the definition of $\tilde{p}_k$ in 16 does not exist.

However, the concept of slant differentiability [16] can be used, and a slanting function $(D\,J_k)^o(v;w_1,w_2)$ may serve as a replacement for the missing second derivative $D^{\,2}J_k(v;w_1,w_2)$ in a so called slant Newton method:

Problem 4. For a given initial guess $v^0 \in V_D$, iterate $v^j \in V_D$ by the rule

$$(D\,J_k)^o\,(v^j\,;\,v^{j+1}-v^j\,,\,w)=-D\,J_k(v^j\,;\,w)\quad\forall w\in V_0\,. \tag{21}$$

Here, a candidate for the slanting function of $D\,J_k$ is given by

$$(D\,J_k)^o\,(v\,;\,w_1,w_2)=\langle\varepsilon(w_1)-\tilde{p}_k{}^o(\varepsilon(v)\,;\,\varepsilon(w_1))\,,\,\varepsilon(w_2)\rangle_{\mathbb{C}}\,, \tag{22}$$

and a candidate for the slanting function p_k in (16) is given by

$$\tilde{p}_k{}^o(\varepsilon(v);\varepsilon(w))=\begin{cases}\frac{2\mu}{2\mu+\sigma_y^2H^2}\left((1-\beta_k)\frac{\langle A_k\,,B\rangle_F}{\|A_k\|_F^2}A_k+\beta_k\,B\right)&\text{if }\beta_k\geq0\,,\\0&\text{else}\,.\end{cases} \tag{23}$$

The above equation uses the abbreviations

$$A_k=A_k(\varepsilon(v))=\operatorname{dev}\tilde{\sigma}_k(\varepsilon(v))\,,\quad B=B(\varepsilon(w))=\operatorname{dev}\varepsilon(w)\,,$$

and the parameter

$$\beta_k=\beta_k(\varepsilon(v))=\frac{\phi_{k-1}(\tilde{\sigma}_k(\varepsilon(v))}{\operatorname{dev}\tilde{\sigma}_k(\varepsilon(v))}\,, \tag{24}$$

with ϕ_{k-1} and $\tilde{\sigma}_k$ as in (17). This parameter is positive in parts of the domain Ω where plastic deformation occurs, and less or equal zero in parts of the domain which behave purely elastic. The interface in between the elastic and plastic zones is called the elastoplastic interface.

Remark 4. The mappings $(D\,J_k)^o$ and p_k^o in (22) and (23) are well defined as slanting functions in the sense of [16] if and only if there exists $\epsilon>0$, such that

$$\phi_{k-1}(\tilde{\sigma}_k(v))\in L_{2+\epsilon}(\Omega)\,. \tag{25}$$

As soon as the variables are discretized, i. e., after Galerkin discretization, the integrability condition (25) is not needed anymore. (see [26, 29]).

Remark 5. The slant Newton method (21) converges locally super-linear, if the mappings in (22) and (23) are slanting functions [16, 29].

2.4 Plain Strain Model

Throughout Section 3, the plain strain model of elastoplasticity is considered, i. e., the domain Ω is assumed to be long and to have a constant shape of the cross section with respect to one of the three directions of the coordinate system. Further, no body forces, traction, or displacements are prescribed in that direction, such that due to symmetry reasons, the solution u_k will vanish in one, let's say the last, component. Therefore it is sufficient to look for a solution u_k in the space $[H^1(\Omega)]^2$ instead of $[H^1(\Omega)]^3$, the domain Ω still has to be considered as a three dimensional object, though.

Consequently, the displacement u and the strain ε, due to (2), read (the time-step index k is now omitted)

$$
u = \begin{pmatrix} u_1(x) \\ u_2(x) \\ 0 \end{pmatrix}, \quad \varepsilon = \begin{pmatrix} \varepsilon_{11} & \varepsilon_{12} & 0 \\ \varepsilon_{12} & \varepsilon_{22} & 0 \\ 0 & 0 & 0 \end{pmatrix}
$$

and the stress σ and plastic strain p, due to (4) and (16), read

$$
\sigma = \begin{pmatrix} \sigma_{11} & \sigma_{12} & 0 \\ \sigma_{12} & \sigma_{22} & 0 \\ 0 & 0 & \sigma_{33} \end{pmatrix}, \quad p = \begin{pmatrix} p_{11} & p_{12} & 0 \\ p_{12} & p_{22} & 0 \\ 0 & 0 & p_{33} \end{pmatrix},
$$

where σ_{33} can be calculated by using σ_{11}, σ_{22}, and σ_{12} (see Table 1), as well as p_{33}, since p is trace free, can be calculated by $p_{33} = -(p_{11} + p_{22})$. Therefore, it is sufficient to represent u, ε, p and σ as the vectors

$$
\mathbf{u} := \begin{pmatrix} u_1 \\ u_2 \end{pmatrix}, \quad \boldsymbol{\varepsilon} := \begin{pmatrix} \varepsilon_{11} \\ \varepsilon_{22} \\ 2\varepsilon_{12} \end{pmatrix}, \quad \mathbf{p} := \begin{pmatrix} p_{11} \\ p_{22} \\ p_{12} \end{pmatrix}, \quad \boldsymbol{\sigma} := \begin{pmatrix} \sigma_{11} \\ \sigma_{22} \\ \sigma_{12} \end{pmatrix},
$$

which is called Voigt's representation. Analogous operations in tensor and vector representation, such as norms, traces and deviators, are summarized in Table 1. Further, in Voigt's representation, there holds $\langle \sigma_\varepsilon \,,\, \varepsilon \rangle_F = \boldsymbol{\sigma}_\varepsilon^T \boldsymbol{\varepsilon}$, and $\langle \sigma_p \,,\, \varepsilon \rangle_F = \boldsymbol{\sigma}_p^T \boldsymbol{\varepsilon}$.

We shall use Voigt's representation throughout the remaining part of this work. Due to that, it is no more necessary to indicate the use of Voigt's representation by bold letters.

Common (Tensor) Representation	Vector Representation
$\varepsilon := \begin{pmatrix} \varepsilon_{11} & \varepsilon_{12} & 0 \\ \varepsilon_{12} & \varepsilon_{22} & 0 \\ 0 & 0 & 0 \end{pmatrix}$	$\boldsymbol{\varepsilon} := \begin{pmatrix} \varepsilon_{11} \\ \varepsilon_{22} \\ 2\,\varepsilon_{12} \end{pmatrix}$
$\sigma_\varepsilon := \mathbb{C}\,\varepsilon = \begin{pmatrix} \sigma_{\varepsilon,11} & \sigma_{\varepsilon,12} & 0 \\ \sigma_{\varepsilon,12} & \sigma_{\varepsilon,22} & 0 \\ 0 & 0 & \sigma_{\varepsilon,33} \end{pmatrix}$ with $\quad \mathbb{C}\,\varepsilon = 2\mu\,\varepsilon + \lambda\,\operatorname{tr}\varepsilon\,I$	$\boldsymbol{\sigma}_\varepsilon := \begin{pmatrix} \sigma_{\varepsilon,11} \\ \sigma_{\varepsilon,22} \\ \sigma_{\varepsilon,12} \end{pmatrix} = \underbrace{\begin{pmatrix} \lambda+2\,\mu & \lambda & 0 \\ \lambda & \lambda+2\,\mu & 0 \\ 0 & 0 & \mu \end{pmatrix}}_{=:C}\,\boldsymbol{\varepsilon}\,,$ $\sigma_{\varepsilon,33} = \underbrace{\dfrac{\lambda}{2\,(\lambda+\mu)}}_{=\nu}\,(1\quad 1\quad 0)\,\boldsymbol{\sigma}_\varepsilon,\ \operatorname{tr}\sigma_\varepsilon = \frac{\nu+1}{\nu}\,\sigma_{\varepsilon,33}$
$\operatorname{dev}\sigma_\varepsilon = \sigma_\varepsilon - \frac{\operatorname{tr}\sigma_\varepsilon}{\operatorname{tr}I}\,I$	$\mathbf{dev}\boldsymbol{\sigma}_\varepsilon := \begin{pmatrix} (\operatorname{dev}\sigma_\varepsilon)_{11} \\ (\operatorname{dev}\sigma_\varepsilon)_{22} \\ (\operatorname{dev}\sigma_\varepsilon)_{12} \end{pmatrix} = \boldsymbol{\sigma}_\varepsilon - \frac{\operatorname{tr}\sigma_\varepsilon}{\operatorname{tr}I}\begin{pmatrix} 1 \\ 1 \\ 0 \end{pmatrix},$ thus, $\mathbf{dev}\boldsymbol{\sigma}_\varepsilon = \underbrace{\left(I - \dfrac{\nu+1}{\dim(\sigma_\varepsilon)}\begin{pmatrix} 1 & 1 & 0 \\ 1 & 1 & 0 \\ 0 & 0 & 0 \end{pmatrix}\right)}_{=:K}\,\boldsymbol{\sigma}_\varepsilon$
$p = \begin{pmatrix} p_{11} & p_{12} & 0 \\ p_{12} & p_{22} & 0 \\ 0 & 0 & -(p_{11}+p_{22}) \end{pmatrix}$	$\mathbf{p} := \begin{pmatrix} p_{11} \\ p_{22} \\ p_{12} \end{pmatrix},\ \|\mathbf{p}\|_N^2 := \mathbf{p}^T \underbrace{\begin{pmatrix} 2 & 1 & 0 \\ 1 & 2 & 0 \\ 0 & 0 & 2 \end{pmatrix}}_{=:N}\,\mathbf{p}\,,$ then: $\quad \|\mathbf{p}\|_N = \|p\|_F$
$\sigma_p := \mathbb{C}\,p = \begin{pmatrix} \sigma_{\varepsilon,11} & \sigma_{\varepsilon,12} & 0 \\ \sigma_{\varepsilon,12} & \sigma_{\varepsilon,22} & 0 \\ 0 & 0 & \sigma_{\varepsilon,33} \end{pmatrix}$ with $\quad \mathbb{C}\,p = 2\,\mu\,p + \lambda\,\underbrace{\operatorname{tr}p}_{=0}\,I = 2\,\mu\,p$	$\boldsymbol{\sigma}_p := \begin{pmatrix} \sigma_{p,11} \\ \sigma_{p,22} \\ \sigma_{p,12} \end{pmatrix} = 2\,\mu\,\mathbf{p}$ and $\quad \sigma_{p,33} = -\,(1\quad 1\quad 0)\,\boldsymbol{\sigma}_p$
$\sigma = \mathbb{C}\,(\varepsilon - p) = \sigma_\varepsilon - \sigma_p$	$\boldsymbol{\sigma} = \boldsymbol{\sigma}_\varepsilon - \boldsymbol{\sigma}_p \quad \text{and} \quad \sigma_{33} = \sigma_{\varepsilon,33} - \sigma_{p,33}$
$\operatorname{dev}\sigma = \operatorname{dev}\sigma_\varepsilon - \underbrace{\operatorname{dev}\sigma_p}_{=\sigma_p}\,,$ $\|\operatorname{dev}\sigma\|_F^2 = \sum_{i,j}(\operatorname{dev}\sigma)_{ij}^2$	$\mathbf{dev}\boldsymbol{\sigma} = \mathbf{dev}\boldsymbol{\sigma}_\varepsilon - \boldsymbol{\sigma}_p\,,\ \|\operatorname{dev}\sigma\|_F = \|\mathbf{dev}\boldsymbol{\sigma}\|_N\,,$ $(\operatorname{dev}\sigma)_{33} = -\,(1\quad 1\quad 0)\,\mathbf{dev}\boldsymbol{\sigma}$

Table 1: Table of Vector Representation regarding the Plain Strain Model.

3 Spatial Discretization

3.1 Galerkin Discretization

We approximate the space $V = [H^1(\Omega)]^2$ by a sequence of finite dimensional subspaces

$$V_{\text{FE}}^1 \subset V_{\text{FE}}^2 \subset \ldots \subset V_{\text{FE}}^{l-1} \subset V_{\text{FE}}^l \subset V_{\text{FE}}^{l+1} \subset \ldots \subset V \,, \tag{26}$$

where V_{FE}^l with $l \in \mathbb{N}$ It is the discrete subspace of V of level l. V_{FE}^l It can be represented by a basis of finite dimension N_l,

$$V_{\text{FE}}^l = \text{span}\{\psi_1, \ldots, \psi_{N_l}\} \,,$$

and let

$$V_{\text{FE},0}^l := V_{\text{FE}}^l \cap V_0, \text{ and } V_{\text{FE},D}^l := V_{\text{FE}}^l \cap V_D \,.$$

Analogously to (21), we have to solve the following discrete problem:

Problem 5. Let $v^0 \in V_{\text{FE},D}^l$ be given, iterate $v^j \in V_{\text{FE},D}^l$, such that

$$(D\,J_k)^o\,(v^j\,;\,v^{j+1} - v^j\,,\,w) = -D\,J_k(v^j\,;\,w) \quad \forall w \in V_{\text{FE},0}^l \,. \tag{27}$$

Remark 6. Differently to the infinite dimensional case, $D\,J_k$ as a mapping from the finite dimensional sets $V_{\text{FE},D}^l \times V_{\text{FE},0}^l$ to $\mathbb{R}$ is slantly differentiable without any extra assumptions (see Remark 4). The slanting function $(D\,J_k)^o$ maps $V_{\text{FE},D}^l \times V_{\text{FE},0}^l \times V_{\text{FE},0}^l$ to $\mathbb{R}$, and is defined as in (22) and (23).

Remark 7. The slant Newton iteration in Problem 5 produces a super-linearly convergent sequence (v_j) [26].

The concept of this subsection is common to all of the following techniques of spatial discretization. However, they differ in the explicit definition of the set $\{\psi_1, \ldots, \psi_{N_l}\}$.

3.2 Low Order FEM (h-FEM)

In this subsection, the reader is assumed to already know the basics of h-FEM (for an introduction on this topic, see [17]). Utilizing this method, we are going to derive the discrete formulas of $D\,J_k$ and $(D\,J_k)^o$ in equation (27), by which Problem 5 finally may be implemented and solved on the computer. Most of this subsection is based on the work [3], and the 2D case (plain strain model) is considered only.

Let $\mathcal{T}$ be a γ-shape regular triangulation of Ω, where all elements $K \in \mathcal{T}$ are triangles. The term γ-shape regular means, that the ratio of diameter

versus radius of the inscribed circle is uniformly bounded from below by a constant $\gamma > 0$ for all elements $K \in \mathcal{T}$.

Let $\mathcal{E} = \{E\}$ denote the set of all edges and $\mathcal{E}_N = \mathcal{E} \cap \Gamma_N$ be its intersection with the Neumann boundary Γ_N. The vertices of all triangles are collected in the set $\mathcal{N} = \{\mathbf{x} \in \mathbb{R}^2 \mid \exists K \in \mathcal{T} : \mathbf{x} \text{ is vertex of } K\}$. Let $\psi_i : \Omega \to \mathbb{R}$ be an affine linear function on each element $K \in \mathcal{T}$ such that for an arbitrary node $\mathbf{x}_l$ the condition $\psi_i(\mathbf{x}_l) = \delta_{il}$ is satisfied for all $i, l \in \{1, \ldots, |\mathcal{N}|\}$. Further, let e_j denote the j-th unit vector. Then, u_{FE} can be expressed by $u_{\mathrm{FE}}(x) := \sum_{i,j} u_{i,j} \psi_i(x) e_j$, where $u_{i,j} := (u(\mathbf{x}_i))_j$, or for short, we can write $u_{\mathrm{FE}}(x) = \Psi(x)^T \mathbf{u}$ by defining $\Psi(x) := (\psi_i(x) e_j)_{i \in \{1,\ldots,|\mathcal{N}|\}, j \in \{1,2\}} \in \mathbb{R}^{2|\mathcal{N}|}$ and $\mathbf{u} := (u_{i,j})_{i \in \{1,\ldots,|\mathcal{N}|\}, j \in \{1,2\}} \in \mathbb{R}^{2|\mathcal{N}|}$. Recalling the notation of Subsection 3.1, the space V is approximated by the subspace $V_{\mathrm{FE}}^l := \{\Psi^T \mathbf{u} \mid \mathbf{u} \in \mathbb{R}^{2|\mathcal{N}|}\}$. Note, that the dimension of the approximation space is $2|\mathcal{N}|$, which is related to the mesh size h by $h \approx \mathcal{N}^{-2}$ in 2D. The term l in V_{FE}^l means, that we have a mesh size of $h = h_0 * 0.5^l$, where h_0 denotes the initial mesh size. In this way, the level l controls the dimension of the approximation space.

Let R_T and R_E be operators which restrict the global vector $\mathbf{u}$ onto a local element T by

$$\mathbf{u}_T = R_T \mathbf{u} , \quad \mathbf{u}_E = R_E \mathbf{u} . \tag{28}$$

Let the fixed triangle $T \in \mathcal{T}$ have the vertices $(\mathbf{x}_\alpha, \mathbf{x}_\beta, \mathbf{x}_\gamma)$ with the coordinates

$$((x_{\alpha,1}, x_{\alpha,2}), (x_{\beta,1}, x_{\beta,2}), (x_{\gamma,1}, x_{\gamma,2})) .$$

Then $\boldsymbol{\varepsilon}(u_{\mathrm{FE}})$ can be calculated on T by

$$\varepsilon(u_h)(\mathbf{x})_{|T} = \begin{pmatrix} \partial_1 \psi_\alpha & 0 & \partial_1 \psi_\beta & 0 & \partial_1 \psi_\gamma & 0 \\ 0 & \partial_2 \psi_\alpha & 0 & \partial_2 \psi_\beta & 0 & \partial_2 \psi_\gamma \\ \partial_2 \psi_\alpha & \partial_1 \psi_\alpha & \partial_2 \psi_\beta & \partial_1 \psi_\beta & \partial_2 \psi_\gamma & \partial_1 \psi_\gamma \end{pmatrix} \begin{pmatrix} u_{\alpha,1} \\ u_{\alpha,2} \\ u_{\beta,1} \\ u_{\beta,2} \\ u_{\gamma,1} \\ u_{\gamma,2} \end{pmatrix} ,$$

or in a more compact way,

$$\varepsilon(u_h)(x)_{|T} = B \, \mathbf{u}_T , \tag{29}$$

where the partial derivatives of ψ_α, ψ_β, and ψ_γ can be obtained by

$$\nabla \begin{pmatrix} \psi_\alpha \\ \psi_\beta \\ \psi_\gamma \end{pmatrix} = \begin{pmatrix} 1 & 1 & 1 \\ x_{\alpha,1} & x_{\beta,1} & x_{\gamma,1} \\ x_{\alpha,2} & x_{\beta,2} & x_{\gamma,2} \end{pmatrix}^{-1} \begin{pmatrix} 0 & 0 \\ 1 & 0 \\ 0 & 1 \end{pmatrix} .$$

13

Integration over body and surface forces may be realized by the midpoint rule. We approximate f_k and g_k by $f_T := f_k(\overline{x}_T)$ and $g_E := g_k(\overline{x}_E)$, where $\overline{x}_T$ and $\overline{x}_E$ denote the center of mass of the element T, and the edge E, respectively. Defining

$$\mathbf{f}_T := \frac{|T|}{3} R_T^T f_T , \quad \text{and} \quad \mathbf{g}_E := \frac{|E|}{2} R_E^T g_E ,$$

on each $T \in \mathcal{T}$ and on each $E \in \mathcal{E}_N$ there hold

$$\int_T f^T v_h \, \mathrm{d}x \approx \mathbf{f}_T^T \mathbf{v} , \quad \text{and} \quad \int_E g^T v_h \, \mathrm{d}s \approx \mathbf{g}_E^T \mathbf{v} . \tag{30}$$

The whole integral over Ω can be split into a sum of integrals on single elements $T \in \mathcal{T}$. Therefore, by combining (28), (29) and (30) we obtain from (18) the discrete formulation of the energy functional's Gâteaux-differential

$$D\, J_k(\mathbf{u} \,;\, \mathbf{v}) := \sum_{T \in \mathcal{T}} \left[|T| \; (C\, B\, \mathbf{u}_T - 2\mu\, \tilde{\mathbf{p}}_k(B\, \mathbf{u}_T))^T B\, R_T - \mathbf{f}_T^T \right] \mathbf{v} - \sum_{E \in \mathcal{E}_N} \mathbf{g}_E^T \mathbf{v}$$

with

$$\tilde{\mathbf{p}}_k(B\, \mathbf{u}_T) := \frac{\max\{0, \phi_{k-1}(\mathbf{dev}\tilde{\boldsymbol{\sigma}}_k(B\, \mathbf{u}_T))\}}{2\mu + \sigma_y^2 H^2} \frac{\mathbf{dev}\tilde{\boldsymbol{\sigma}}_k(B\, \mathbf{u}_T)}{\|\mathbf{dev}\tilde{\boldsymbol{\sigma}}_k(B\, \mathbf{u}_T)\|_N} + \mathbf{p}_{k-1} , \tag{31}$$

where

$$\mathbf{dev}\tilde{\boldsymbol{\sigma}}_k(B\, \mathbf{u}_T) \quad := \quad KCB\, \mathbf{u}_T - 2\,\mu\, \mathbf{p}_{k-1} , \tag{32}$$
$$\phi_{k-1}(\mathbf{dev}\tilde{\boldsymbol{\sigma}}_k(B\, \mathbf{u}_T)) \quad := \quad \|\mathbf{dev}\tilde{\boldsymbol{\sigma}}_k(B\, \mathbf{u}_T)\|_N - \sigma_y(1 + H\alpha_{k-1}) . \tag{33}$$

Since $D\, J_k(\mathbf{u} \,;\, \mathbf{v})$ is linear in $\mathbf{v}$, there exists the Fréchet-derivative

$$D\, J_k(\mathbf{u}) = \sum_{T \in \mathcal{T}} \left(|T| \; (CB\, \mathbf{u}_T - 2\mu\, \tilde{\mathbf{p}}_k(B\, \mathbf{u}_T))^T B\, R_T - \mathbf{f}_T \right) - \sum_{E \in \mathcal{E}_N} \mathbf{g}_E . \tag{34}$$

The mapping $D\, J_k$ is slantly differentiable with

$$(D\, J_k)^o\, (\mathbf{u}) = \sum_{T \in \mathcal{T}} |T| \; R_T^T B^T (C - 2\mu\, \tilde{\mathbf{p}}_k^o(B\, \mathbf{u}_T))^T B\, R_T ,$$

where

$$\tilde{\mathbf{p}}_k^o(B\, \mathbf{u}_T) = \begin{cases} \xi \left((1 - \beta_k) \frac{\mathbf{dev}\tilde{\boldsymbol{\sigma}}_k \mathbf{dev}\tilde{\boldsymbol{\sigma}}_k^T N}{\|\mathbf{dev}\tilde{\boldsymbol{\sigma}}_k\|_N^2} + \beta_k I \right) KC & \text{if } \phi_k(\tilde{\boldsymbol{\sigma}}_k) > 0 , \\ 0 & \text{else} . \end{cases} \tag{35}$$

serves as a slanting function for $\tilde{\mathbf{p}}_k$ defined in (31). Here, the definitions $\xi := \frac{1}{2\mu+\sigma_y^2 H^2}$ and $\beta_k := \frac{\phi_{k-1}(\mathbf{dev}\tilde{\boldsymbol{\sigma}}_k)}{\|\mathbf{dev}\tilde{\boldsymbol{\sigma}}_k\|_N}$, and the abbreviation $\mathbf{dev}\tilde{\boldsymbol{\sigma}}_k$ for $\mathbf{dev}\tilde{\boldsymbol{\sigma}}_k(B\,\mathbf{u}_T)$ as in (32) are used.

The Newton-like method is applied for the calculation of $\mathbf{u} \in \mathbb{R}^{2|\mathcal{N}|}$ such that $DJ_k(\mathbf{u}) = 0$ and $\mathbf{u}$ satisfies the Dirichlet boundary condition:

$$\mathbf{u}_i = \mathbf{u}_{i-1} + \Delta\mathbf{u}_i \qquad (\forall i \in \mathbb{N}), \tag{36}$$

where $\Delta\mathbf{u}_i$ solves

$$-\left(D\,J_k\right)^o(\mathbf{u}_{i-1})\,\Delta\mathbf{u}_i = D\,J_k(\mathbf{u}_{i-1})\ .$$

Note, that $\mathbf{u}_i$ must satisfy (generally inhomogeneous) Dirichlet boundary conditions for all $i \in \mathbb{N}$. Therefore, it is sufficient for the initial approximation $\mathbf{u}_0$ to satisfy the inhomogeneous Dirichlet conditions, and for $\Delta\mathbf{u}_i$ to solve the homogeneous Dirichlet conditions.

3.3 High Order FEM (p-FEM)

In this section, we will briefly mention the most important definitions and results of high order Finite Element Methods (p-FEM). For more detailed information, the interested reader is referred to the pioneering work [8], and the monograph [45]. Same as in h-FEM, also in p-FEM a γ-shape regular mesh is used, but in contrast to h-FEM, the accuracy of the approximate solution is increased, i. e., the dimension of the finite element space V_{FE}^l is enlarged, by increasing the polynomial degree of the shape functions instead of refining the mesh by the partitioning of elements. The big advantage of a high order method is the faster convergence [7], whereas the major drawback of a high order method is the expensive assembling of the system matrix. As long as this handicap can be settled (e.g., by finding recurrences via symbolic computation [9, 11, 12]), the application of such methods are definitely worth their price. We turn to the basic definition of hierarchic basis functions in p-FEM. Let be mentioned, that in this paper, we concentrate on the Karniadakis-Sherwin polynomials [32]. Before defining the discretization of the vector valued displacement field $u \in \left[H^1(\Omega)\right]^2$, the scalar case $u \in H^1(\Omega)$ is discussed.

Let the reference triangle $\hat{K}$ and the reference square $\hat{Q}$ be defined by

$$\hat{K} := \{(x,y) \mid x > -1,\, y > -1,\, x + y < 0\} \quad \text{and} \quad \hat{Q} = (-1,1)^2\,. \tag{37}$$

The Duffy transformation $D : \mathbb{R}^2 \to \mathbb{R}^2$, defined by

$$D(\eta_1, \eta_2) = \left(\frac{1}{2}(1+\eta_1)(1-\eta_2) - 1\ ,\ \eta_2\right), \tag{38}$$

15
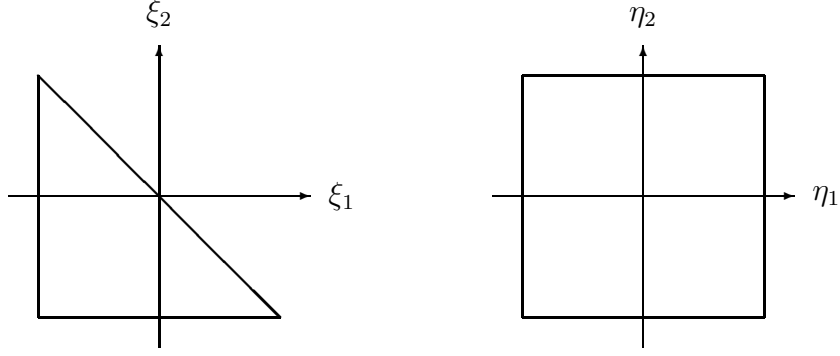
Figure 1: The reference elements $\hat{K}$ and $\hat{Q}$ defined in equation (37).

maps $\hat{Q}$ onto $\hat{K}$. The inverse maps $\hat{K}$ onto $\hat{Q}$ and is given by

$$D^{-1}(\xi_1, \xi_2) = \left(2\frac{1+\xi_1}{1-\xi_2} - 1 \ , \ \xi_2\right) .$$

The further proceeding is to define local shape functions Φ on $\hat{Q}$ and then, by the application of the inverse Duffy transformation $\Psi = \Phi \circ D^{-1}$, to obtain local shape functions on the reference triangle $\hat{K}$.

Definition 1. Let $\alpha > -1$, $\beta > -1$, and $n \in \mathbb{N} \cup \{0\}$ be given. The polynomial $P_n^{(\alpha,\beta)} : [-1, 1] \to \mathbb{R}$ defined by

$$P_n^{(\alpha,\beta)}(\eta) := \frac{(-1)^n}{2^n\, n!}\, (1-\eta)^{-\alpha}(1+\eta)^{-\beta}\, \frac{d^n}{d\eta^n}\left((1-\eta)^{\alpha+n}(1+\eta)^{\beta+n}\right) \quad (39)$$

is called nth *Jacobi Polynomial with respect to the weight* $(1-\eta)^{\alpha}(1+\eta)^{\beta}$.

Definition 2. Let the reference elements $\hat{K}$ and $\hat{Q}$ be given by (37) and let the transformation $D : \mathbb{R}^2 \to \mathbb{R}^2$ be defined as in (38). For a given polynomial degree $p \in \mathbb{N}$ we define the set $\Psi = \bigcup_{B=1}^{5} \Psi^B$ of local shape functions by

$$\Psi^B := \Phi^B \circ D^{-1} = \{\phi \circ D^{-1} \mid \phi \in \Phi^B\} \quad B = 1, \ldots, 5, \quad (40)$$

where Φ^B is given by:

$$
\begin{aligned}
\Phi^1 &= \{\frac{(1-\eta_1)}{2}\frac{(1-\eta_2)}{2}, \frac{(1+\eta_1)}{2}\frac{(1-\eta_2)}{2}, \frac{(1+\eta_2)}{2}\}, \\
\Phi^2 &= \{\frac{(1-\eta_1)}{2}\frac{(1+\eta_1)}{2}\frac{(1-\eta_2)}{2}P_{i-1}^{(1,1)}(\eta_1) \mid i = 1,\ldots,p-1\}, \\
\Phi^3 &= \{\frac{(1+\eta_1)}{2}\frac{(1-\eta_2)}{2}\frac{(1+\eta_2)}{2}P_{i-1}^{(1,1)}(\eta_2) \mid i = 1,\ldots,p-1\}, \\
\Phi^4 &= \{\frac{(1-\eta_1)}{2}\frac{(1-\eta_2)}{2}\frac{(1+\eta_2)}{2}P_{i-1}^{(1,1)}(\eta_2) \mid i = 1,\ldots,p-1\}, \\
\Phi^5 &= \{\frac{(1-\eta_1^2)}{4}\frac{(1+\eta_2)}{2}\frac{(1-\eta_2)^{i+1}}{2^{i+1}}P_{i-1}^{(1,1)}(\eta_1)P_{j-1}^{(2i+1,1)}(\eta_2) \\
&\qquad\qquad\qquad\qquad\qquad \mid i,j = 1,\ldots,p-1\}.
\end{aligned}
$$

The subdivision of the shape functions is as follows: The set Φ^1 contains vertex shape functions, which vanish on all vertices, except on one, where the value one is attained. The set Φ^5 contains the interior bubble functions, which vanish on all edges, and the remaining sets Φ^2, Φ^3, Φ^4 contain edge bubble functions, which vanish on all but one edge. In [32] it is shown, that Ψ is a set of linear independent polynomial functions, and that the span of Ψ contains all polynomials of degree p an the reference triangle $\hat{K}$.

In this way we approximate $u \in H^1(\Omega)$ by $u_{\mathrm{FE}} \in S^p(\Omega, \mathcal{T})$ with

$$
S^p(\Omega, \mathcal{T}) := \{u \in H^1(\Omega) \mid u \circ F_K \in \mathrm{span}\Psi \text{ for all } K \in \mathcal{T}\}, \qquad (41)
$$

where F_K denotes the mapping from the reference triangle $\hat{K}$ to the local element K. In case of vector valued problems, such as in elastoplasticity, each shape function $\psi \in \Psi$ is replaced by a set of d vector valued shape functions $\{\psi\, e_i \mid i = 1,\ldots,d\}$, where e_i denotes the ith unit vector. Speaking in the notation of Subsection 3.1, we have $V_{FE}^l = S^{p_l}(\Omega, \mathcal{T})$, where p_l denotes the polynomial degree of level l. In order to keep the property (26), one has to guarantee $p_l \geq p_{l-1}$.

The a priori error analysis of the high order Finite Element Method [7] states the convergence $(d = 2)$

$$
\|u - u_{\mathrm{FE}}\|_{H^1(\Omega)} \leq C\, p^{-s}\, \|u\|_{H^{s+1}(\Omega)}
$$

if $u \in H^{s+1}(\Omega)^2$, and in the case of singular behavior of the type $u \approx r^\alpha$, $\alpha > 0$, where r is the distance from the singularity, we obtain

$$
\|u - u_{\mathrm{FE}}\|_{H^1(\Omega)} \leq C\, p^{-2\alpha},
$$

which is twice the rate of the h-version.

3.4 Combining Low and High Order FEM (hp-FEM)

The concept of hp-FEM is the adaptive combination h-FEM and p-FEM. The key idea is to increase the polynomial degree locally on elements, where the solution has high regularity. On such elements we can expect locally up to exponential convergence (see [5, 45]) of the approximate towards the solution, On other elements, where the regularity of the solution is low, mesh refinement, i. e. h-FEM, is applied, which locally yields algebraic convergence. Globally, the convergence of hp-approximations is much faster than the convergence in h-FEM or p-FEM, under certain conditions up to exponential convergence can be achieved. The price we pay is, that the method is much harder to implement than h- or p-FEM. We turn to the definition of the approximation space, which actually will be very much the same as in p-FEM.

Let a polynomial degree $p_K \in \mathbb{N}$ be associated with each element $K \in \mathcal{T}$ and the polynomial degree p_e with each edge e by

$$p_e = \min\{p_K \mid e \text{ is an edge of } K\}.$$

The information of polynomial degree distribution is collected in a vector $\mathbf{p} = (p_K)_{K \in \mathcal{T}}$, which is called (polynomial) degree vector.

With p_{Ke1}, p_{Ke2}, p_{Ke3}, and p_K denoting the polynomial degree on the edges e_1, e_2, e_3, and in the interior of element K, the set of shape functions Ψ is defined as in Definition 2, where $\Phi^1, \ldots, \Phi^5$ are given by:

$$\Phi^1 = \{\frac{(1-\eta_1)}{2}\frac{(1-\eta_2)}{2}, \frac{(1+\eta_1)}{2}\frac{(1-\eta_2)}{2}, \frac{(1+\eta_2)}{2}\},$$

$$\Phi^2 = \{\frac{(1-\eta_1)}{2}\frac{(1+\eta_1)}{2}\frac{(1-\eta_2)}{2}P_{i-1}^{(1,1)}(\eta_1) \mid i = 1, \ldots, p_{AB} - 1\},$$

$$\Phi^3 = \{\frac{(1+\eta_1)}{2}\frac{(1-\eta_2)}{2}\frac{(1+\eta_2)}{2}P_{i-1}^{(1,1)}(\eta_2) \mid i = 1, \ldots, p_{BC} - 1\},$$

$$\Phi^4 = \{\frac{(1-\eta_1)}{2}\frac{(1-\eta_2)}{2}\frac{(1+\eta_2)}{2}P_{i-1}^{(1,1)}(\eta_2) \mid i = 1, \ldots, p_{CA} - 1\},$$

$$\Phi^5 = \{\frac{(1-\eta_1^2)}{4}\frac{(1+\eta_2)}{2}\frac{(1-\eta_2)^{i+1}}{2^{i+1}}P_{i-1}^{(1,1)}(\eta_1)P_{j-1}^{(2i+1,1)}(\eta_2)$$
$$\mid i,j = 1, \ldots, p_K - 1\}.$$

The approximation space reads

$$S^{\mathbf{p}}(\Omega, \mathcal{T}) := \{u \in H^1(\Omega) \mid u \circ F_K \in \text{span}\Psi \text{ for all } K \in \mathcal{T}\}, \qquad (42)$$

where Ψ depends on p_{Ke1}, p_{Ke2}, p_{Ke3}, and p_K. Referring to Subsection 3.1, in hp-FEM the approximation space is defined $V_{FE}^l = S^{\mathbf{p}_l}(\Omega, \mathcal{T})$, where $\mathbf{p}_l$

denotes the polynomial degree vector of level l. In order to keep the property (26), one has to guarantee $\mathbf{p}_l \geq \mathbf{p}_{l-1}$ component wise.

As already mentioned, the hp-method is expensive, but the approximation converges very fast. It is even possible to achieve exponential convergence, if the solution is analytic up to point-wise singularities on the boundary (if $\Omega \in \mathbb{R}^2$). Therefore the construction of ideal geometric meshes and the use of linear degree vectors (see Definitions 3 and 4), is assumed. However, in such cases the convergence rate is globally even exponential ([6], [45, Theorem 4.63])

$$\|u - u_{FE}\|_{H^1(\Omega)} \leq C \exp(-bN^{1/3}),\qquad(43)$$

where C and b denote some positive constants, and $N = \dim(S^{\mathbf{p}}(\Omega, \mathcal{T}))$ denotes the dimension of the used finite element space.

In elastoplasticity, the solution in each time step is known to be in $H^2_{\mathrm{loc}}(\Omega)$, and analytic in balls where the plastic strain p vanishes [36, 10]. These, so called elastic zones, typically cover the major part of the domain Ω, thus, the application of an hp-FEM is a natural choice. In those parts of the interior domain, where the material reacts purely elastic, the polynomial degree of the shape functions is increased, whereas the mesh is being h-refined in plastic areas and towards rough boundary data or geometry.

Whenever plastic zones are small compared to elastic zones, the application of hp-FEM is worth the cost. However, since the plastic zones are a set of non-zero measure, we cannot expect an exponential convergence rate as in (43), but some algebraic convergence which is faster than in both h-FEM and p-FEM.

The basic hp-adaptive algorithm reads as presented in Algorithm 1.

Algorithm 1 The hp-adaptive Algorithm:

Require: A mesh $\mathcal{T}$, a polynomial degree vector $(p_K)_{K \in \mathcal{T}}$, a Finite Element Solution u_{FE}.

Ensure: A refined mesh $\mathcal{T}_{\mathrm{ref}}$, a new polynomial degree vector $(p_K)_{K \in \mathcal{T}_{\mathrm{ref}}}$.

1: Determine which elements to refine $\rightarrow \mathcal{T}_h$.
2: Determine where the polynomial degree should be increased $\rightarrow \mathcal{T}_p$.
3: Obtain a preliminary refined mesh $\rightarrow \mathcal{T}'_{\mathrm{ref}}$.
4: Elimination of hanging nodes $\rightarrow \mathcal{T}_{\mathrm{ref}}$.
5: Increase the polynomial degree $p_K = p_K + 1$ for all elements $K \in \mathcal{T}_{\mathrm{ref}} \cap \mathcal{T}_p$. In particular: Elements to which an h-refinement is applied inherit the polynomial degree from their father.

Note, that Items 3–5 are straight forward, whereas, one still has to decide on the exact realization of Items 1 and 2. In general, the set of all

adaptive strategies divides into two classes: strategies which are problem dependent, and those which are not. In problem dependent strategies, the decision whether to refine in h, or in p, or not at all, relies on the evaluation of problem dependent quantities, typically the error estimator. Strategies of this type can be found in [42, 18, 1].

Due to the lack of a reliable and efficient error estimator for elastoplasticity, the use of problem independent algorithms is a natural choice. Methods as in [20, 21], estimate the regularity of the solution without using problem dependent quantities. The main idea of these strategies is to minimize a local error projection of a reference solution, that is obtained by a uniformly h-refined mesh intermediately. In this way an optimal hp-mesh is produced adaptively. The big advantage of such method is, that no knowledge about the problem has to be passed to the mesh generation, the drawback is to cope with different meshes at the same time, which often is hard to implement on the computer in Finite Element frameworks.

In this paper we choose a strategy of hp-refinement, which is presented in [23]. This strategy was first discussed in [38] for the spectral element method, and later used in [30] for hp-FEM in one dimension (or in more dimensions, where elements have tensor structure). T. Eibner and M. Melenk [23] present the extension of the strategy to hp-FEM for the Poisson problem in more dimensions, i. e., where elements have the shape of triangles and tetrahedrons. Especially two advantages are covered by this approach: First, the algorithm is problem independent (see Remark 8), and second, there is no need to handle more than one FE-mesh in the implementation. The algorithm is based on the estimating the Sobolev regularity of the solution by a certain L_2-orthogonal polynomial expansion:

Proposition 1. *Define on the reference triangle $\hat{K}$ the $L_2(\hat{K})$-orthogonal basis ψ_{pq}, $p, q \in \mathbb{N}_0$ by*

$$\psi_{pq} = \tilde{\psi}_{pq} \circ D^{-1}, \quad \tilde{\psi}_{pq} = P_p^{(0,0)}(\eta_1) \left(\frac{1 - \eta_2}{2} \right)^p P_q^{(2p+1,0)}(\eta_2),$$

where $P_p^{(\alpha,\beta)}$ is the (well known) p-th Jacobi polynomial with respect to the weight $\eta \mapsto (1-\eta)^\alpha (1+\eta)^\beta$ and D the Duffy transformation. Let $u \in L_2(\hat{K})$ be written as

$$u = \sum_{p,q \in \mathbb{N}_0} u_{pq} \psi_{pq}. \tag{44}$$

Then u is analytic on $\overline{\hat{K}}$ if and only if there exist constants $C, b > 0$ such that $|u_{pq}| \leq C\, e^{-b(p+q)}$ for all $p, q \in \mathbb{N}_0$.

Proof. See [39]. $\qquad\square$

Since the true solution u is not available, the idea for an hp-adaptive algorithm is to estimate the decay of the coefficients u_{pq} of the L_2 conforming expansion of the finite element solution $u_{FE|K} \circ F_K = \sum_{p,q} u_{pq} \psi_{pq}$ instead. If the decay is exponentially, then the polynomial degree p will be increased, otherwise, the mesh will be refined, see Algorithm 2.

Algorithm 2 Items 1 and 2 in Algorithm 1:

Require: A mesh $\mathcal{T}$; a polynomial degree vector $(p_K)_{K \in \mathcal{T}}$; parameters $b > 0$ and $\sigma \geq 0$; a Finite Element Solution u_{FE}; a reliable, efficient, and localizable a posteriori error estimator $\eta(u_{\mathrm{FE}})$.

Ensure: The marked elements $\mathcal{T}_p$ and $\mathcal{T}_h$.

1: Compute the mean error $\bar{\eta}^2 = |\mathcal{T}|^{-1} \sum_{K \in \mathcal{T}} \eta_K^2$
2: For elements $K \in \mathcal{T}$ with $\eta_K^2 \geq \sigma \bar{\eta}^2$ compute the expansion coefficients

$$u_{ij,K} = \|\psi_{ij}\|_{L_2(\hat{K})}^{-2} \, \langle u_{\mathrm{FE}|K} \circ F_K \,, \, \psi_{ij} \rangle_{L_2(\hat{K})}$$

for $0 \leq i + j \leq p_K$.
3: Estimate the decay coefficient b_K by a least squares fit of

$$\ln|u_{ij,K}| \approx C_K - b_K(i + j)\,.$$

4: Determine

$$\mathcal{T}_p = \{K \in \mathcal{T} \mid \eta_K^2 \geq \sigma \bar{\eta}^2 \wedge b_K \geq b\}\,,$$
$$\mathcal{T}_h = \{K \in \mathcal{T} \mid \eta_K^2 \geq \sigma \bar{\eta}^2 \wedge b_K < b\}\,.$$

Remark 8. Note, that in the above algorithm, the use of an a-posteriori error estimator can be switched off by setting $\sigma = 0$. The crucial part of the algorithm is testing the approximated slope of the expansion coefficients versus a given critical slope b. In this sense, the algorithm is problem independent, the use of an a-posteriori error estimator may nevertheless be of advantage.

In Section 4 we compare Algorithm 2 with a standard hp-adaptive approach, which is proposed a Series of papers by L. Demkowicz, T. Oden, W. Rachowicz, and coworkers [19, 41, 43] and also used in hp-BEM, e. g., [28]. This approach, summarized in Algorithm 3, puts the decision of whether refining in h or in p solely on the local evaluation of an a-posteriori-error-estimator $\eta_K(u_{\mathrm{FE}})$.

Algorithm 3 Items 1 and 2 in Algorithm 1:
___
Require: A mesh $\mathcal{T}$; parameters $0 < \sigma_1 < \sigma_2 < 1$; a localizable a-posteriori error estimator $\eta(u_{\mathrm{FE}})$.
Ensure: The marked elements $\mathcal{T}_p$ and $\mathcal{T}_h$.

  1: Compute the maximum error $\eta_{\max} = \max_{K \in \mathcal{T}} \eta_K$
  2: Determine

$$\mathcal{T}_p = \{ K \in \mathcal{T} \mid \sigma_1 \, \eta_{\max} < \eta_K \leq \sigma_2 \, \eta_{\max} \},$$
$$\mathcal{T}_h = \{ K \in \mathcal{T} \mid \sigma_2 \, \eta_{\max} < \eta_K \}.$$

3.5 The Zone Concentrated FEM

In addition to the *hp*-adaptive strategy in Algorithm 1, we investigate also another approach, which we call a Zone Concentrated FEM (ZC-FEM). For this technique we use the knowledge of Boundary Concentrated FEM (BC-FEM, [33]). This approach is still of an *hp*-adaptive Finite Element type, but with a slightly different aim:

Let us start with a short review on BC-FEM: Considering the regularity of the solution to be low at the boundary and high in the interior of the domain, the parameters h and p are chosen to be small in a neighbourhood of the boundary and to be growing towards the interior of the domain. This growth is based on the use of *geometric meshes* and *linear polynomial degree vectors*, which are defined as follows:

Definition 3. A γ-shape-regular mesh $\mathcal{T}$ is called a geometric mesh with boundary mesh size h if there exist constants c_1, $c_2 > 0$ such that for all $K \in \mathcal{T}$ with diameter h_K the following hold:

  1. $h \leq h_K \leq c_2 h$ at the boundary, and

  2. $c_1 \inf_{x \in K} \overline{(x, \Gamma)} \leq h_K \leq c_2 \sup_{x \in K} \overline{(x, \Gamma)}$.

Here, $\overline{(x, \Gamma)}$ denotes the shortest distance of point x to the boundary $\Gamma = \partial \Omega$.

Definition 4. A polynomial degree vector $\mathbf{p} := (p_K)_{K \in \mathcal{T}}$ is said to be *linear* with slope $\alpha > 0$ if there exist positive constants c_1 and c_2, such that

$$1 + \alpha \, c_1 \, \log \frac{h_K}{h} \leq p_K \leq 1 + \alpha \, c_2 \, \log \frac{h_K}{h} \, .$$

holds for all $K \in \mathcal{T}$.

In BC-FEM, a *hp*-FEM discretization is performed, which uses a geometric mesh $\mathcal{T}$ and a linear polynomial degree vector **p**. If the slope α of Definition 4 is chosen large enough, then the convergence rate of BC-FEM is of the same order as in *h*-FEM, namely in 2D

$$\|u - u_{FE}\|_{H^1(\Omega)} \leq \|u\|_{H^{1+s}(\Omega)} h^s,$$

where u is assumed to have global Sobolev regularity $u \in [H^{1+s}(\Omega)]^2$ with $s \in (0, 1)$, and h denotes the mesh size on the boundary.

Note, that the number of unknowns is significantly smaller than in *h*-FEM. namely, in BC-FEM the number of unknowns is proportional to the number of unknowns on the boundary (such as in BEM), whereas in a classical *h*-FEM the number of degrees of freedom is proportional to the *square* of the number of unknowns on the boundary. This is why the method is called a Boundary Concentrated Finite Element Method (BC-FEM) [33]. And this is the conceptional difference to other *hp*-adaptive strategies: The method exploits the knowledge about the regularity of the solution in a way, that it searches for the smallest (and sparse) system which allows for the same convergence rate as is obtained in a uniform *h*-FEM.

Here we come to the extension of BC-FEM, which we call ZC-FEM: In elastoplasticity, BC-FEM can be applied for the purely elastic region, where the solution is known to be analytic [10], whereas the plastic region, where the solution is known to be just in H^2_{loc} [36], is discretized by using a classical *h*-FEM. Usually, when applying BC-FEM, the geometric mesh $\mathcal{T}$, and the linear polynomial degree vector **p** can be constructed in advance, since the position of the boundary is known. This is different when using ZC-FEM for elastoplastic problems. The interface between plastic and elastic parts of the domain, which represents a part of the boundary of the elastic zone, is not known in advance. This is due to the fact that the calculation of the plastic strain field relies on the solution of the problem (the displacement field), as it is pointed out in equation (16). In other words, after every refinement step the interface will probably move. Thus, one has to estimate, which parts of the domain will be plastic at the next step of refinement. This task can be handled by two different strategies:

The first is to test the analyticity of the FE-solution as presented in Algorithm 2 (with $\sigma = 0$). This would yield an optimal prediction of the plastic zones in the next step of refinement. Although, the prize we pay is a fairly high-dimensional test situation, since the polynomial degree of the shape functions has to be high (experimentally: greater than 4) in order to obtain a reasonable prediction of the plastic zones.

The second option is to mark all elements for *h*-refinement, if they behave plastic at this level of refinement, i. e., where the plastic strain p_k yields

$\|p_k\|_{L_2(K)} > 0$, and additionally mark elements for h-refinement, which have a common vertex with those. This technique implicitly assumes, that the elastoplastic interface of the FE-solution after the refinement will move no further than at most one layer of elements from its former position.

The resulting method has the same accuracy as a classical h-FEM, i.e. $\|u - u_{\mathrm{FE}}\|_{H^1(\Omega)} = O(h)$, but the number of degrees of freedom is significantly smaller: Considering h-FEM in two dimensions $(d = 2)$, the number degrees of freedom is roughly $O(N^2)$, with $N = h^{-1}$ denoting the number of nodes on the boundary of the domain, whereas in BC-FEM it is $O(N_E) + O(N_P^2)$, where N_E is the number of nodes on the boundary of the purely elastic sub-domain, and N_P the number of nodes on the boundary of the plastic sub-domain. Thus, this method pays off in situations, where the area of the plastic regions is small compared to the overall domain.

4   Numerical Examples

We discuss three different numerical examples, for each of which a uniform h-FEM and four different hp-adaptive FEM strategies are performed:

- *Strategy 1* is a Zone Concentrated FEM as outlined in Subsection 3.5. It is the combination of a-priori h-refinement towards the boundary and the plastic zones. An element is treated as a part of the plastic zone, if one of its vertices belongs to an element, where the plastic strain is nonzero, $\|p_k\|_F \neq 0$. The remaining part of the domain, which reacts purely elastic, is discretized by a geometric mesh and a linear polynomial degree vector (see Definition 3 and 4).

- *Strategy 2* exactly recovers Algorithm 2, where the parameters are set to $\sigma = 10^{-4}$ and $b = 3$. If the FE-solution is of too low order $(p < 5)$ locally, then testing for analyticity is not reliable, and the element is marked for p-refinement.

- *Strategy 3* is almost identical to *Strategy 2*, and also using the same parameters. In difference to *Strategy 2*, plastic elements (where the plastic strain p_k yields $\|p_k\|_F \neq 0$) are marked for h-refinement in advance. Also elements, which have a common vertex with those, are marked for h-refinement, since the elastoplastic interface may move from refinement to refinement. This way, the polynomial degree of the FE-solution may kept low in elastoplastic zones.

- *Strategy 4* is the classical hp-adaptivity approach, as in Algorithm 3. The parameters are set to $\sigma_1 = 10^{-8}$ and $\sigma_2 = 10^{-4}$.

Remark 9. In all of the above Strategies, which rely on a-posteriori error-estimation, the ZZ-error-estimator

$$\eta_K^2(u_{\text{FE}}) = \int_K (\sigma_{\text{FE}} - \sigma_{\text{FE}}^*) : \mathbb{C}^{-1}(\sigma_{\text{FE}} - \sigma_{\text{FE}}^*) \, \mathrm{d}x \, ,$$

$$\eta^2(u_{\text{FE}}) = \frac{\sum_{K \in \mathcal{T}} \eta_K^2}{\sum_{K \in \mathcal{T}} \int_K \sigma_{\text{FE}}^* : \mathbb{C}^{-1}\sigma_{\text{FE}}^* \, \mathrm{d}x} \tag{45}$$

is used. Here, the flux $\sigma_{\text{FE}} = \mathbb{C} \, \varepsilon(u_{\text{FE}})$ is the elastic part of the stress depending on the finite element solution u_{FE} (element wise), and σ_{FE}^* is the Clement Interpolation of σ_{FE}. This error estimator is known to be reliable for elastoplastic problems with hardening [4]. However, this error estimator is not efficient, thus not equilibrated. To the best of the author's knowledge, there is no equilibrated a-posteriori error-estimator known for elastoplasticity.

All examples were computed in the framework NETGEN/NGSolve [44].

Example 1. A beam $\Omega = (0, 2) \times (-0.5, 0.5)$ is fixed on the left boundary $\Gamma_D = \{(x, y) \in \partial\Omega \mid x = 0\}$ and stressed on the right boundary $\Gamma_N = \{(x, y) \in \partial\Omega \mid x = 2\}$ in positive x-direction with a traction of intensity $|g| = 1.35$ (see Figure 2). The material parameters are chosen as follows: Young's modulus $E = 1000$, Poisson ratio $\nu = 0.3$, yield stress $\sigma_y = 1$, and modulus of hardening $H = 10$. The graphical output after some steps of uniform refinement is as follows: The displacement is plotted in Figure 3, which also shows the deformation of the domain magnified by a factor 100. The yield function ϕ (8) is plotted in Figure 4. In Figure 5 the plastic zones (red) versus elastic zones (blue) are shown, whereas Figure 6 and Figure 7 report on the point-wise Frobenius-norm of the plastic strain. The estimated slope of the FE solution coefficients, as discussed in Algorithm 2, is plotted in Figure 8. We numerically tested uniform refinement (h-FEM) versus the hp-FE Strategies 1-4. Let be mentioned, that in all tests the super linear convergence of the Newton like method was observed. Figures 9-12 illustrate the polynomial order distribution after some steps of adaptive hp-refinement, whereas the resulting meshes are shown in Figures 13-16. The approximation error $\|u - u_{\text{FE}}\|_{H^1(\Omega)}$ is estimated by the elastic ZZ-error estimator (45). Figures 17 and 18 show the convergence results graphically.
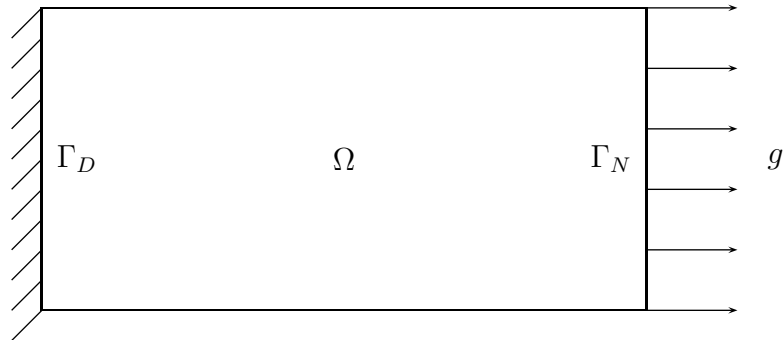
Figure 2: Geometry and problem description of Example 1.
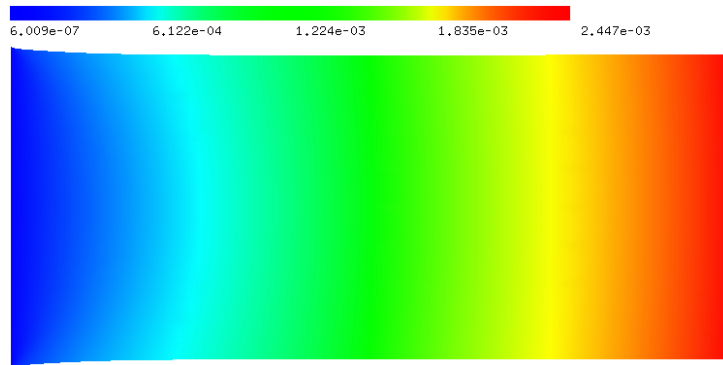
Figure 3: Displacement and deformed domain ($\times 100$) in Example 1.
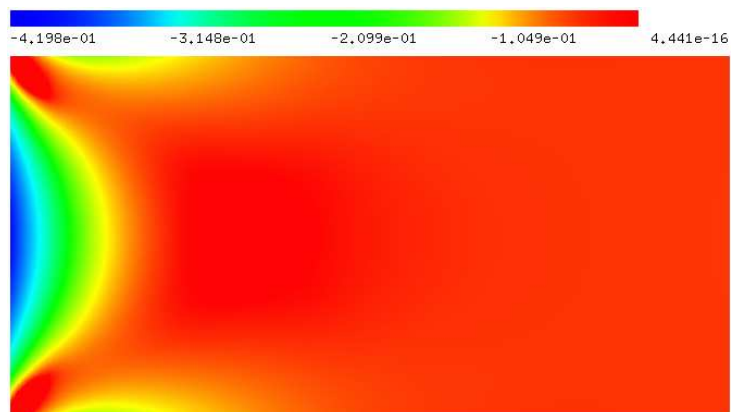

Figure 4: Yield function ϕ (8) in Example 1.

26
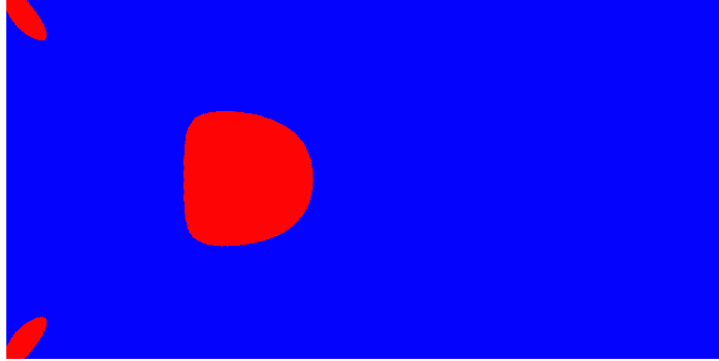
Figure 5: Plastic (red) and elastic (blue) zones in Example 1.
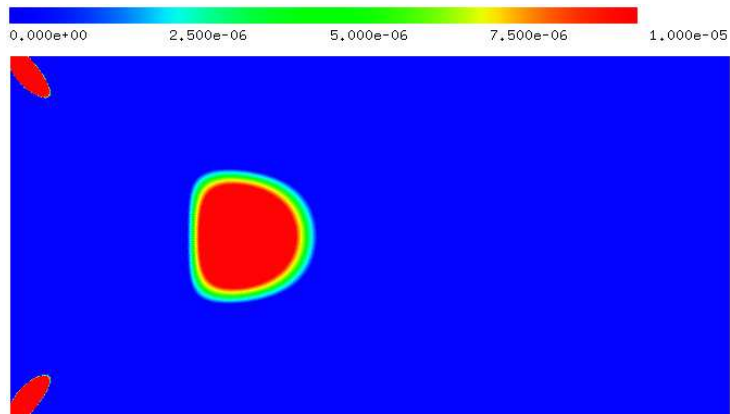

Figure 6: Frobenius norm of the plastic strain in Example 1.
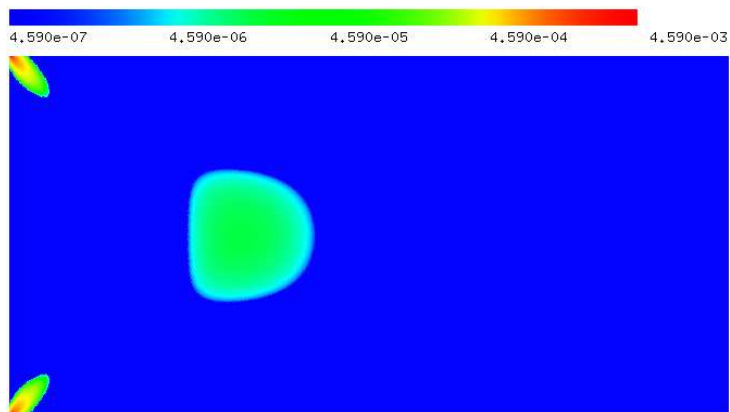

Figure 7: Logarithmic Frobenius norm of the plastic strain in Example 1.

27
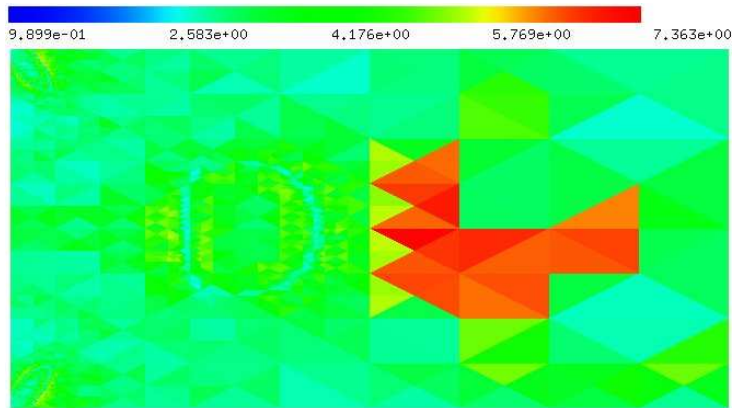
Figure 8: The estimated slope of coefficients (Algorithm 2) in Example 1.
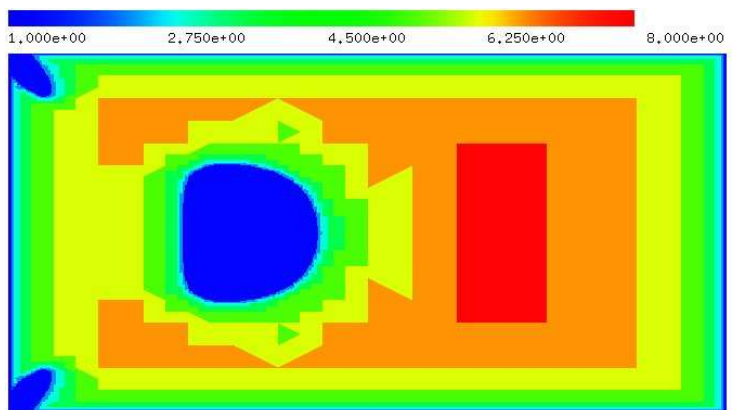
Figure 9: Polynomial order with Strategy 1 in Example 1.
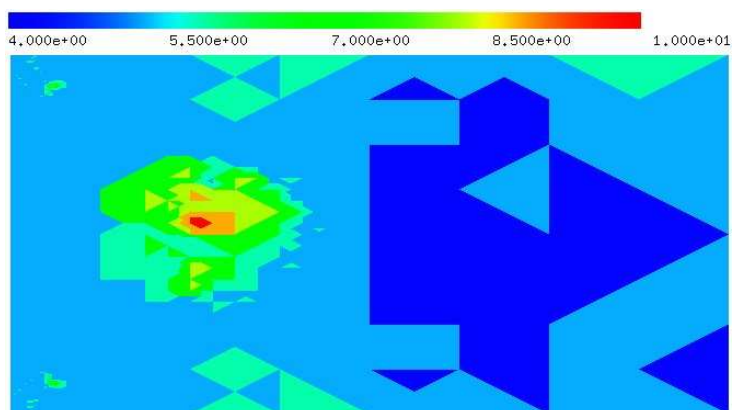
Figure 10: Polynomial order with Strategy 2 in Example 1.

28
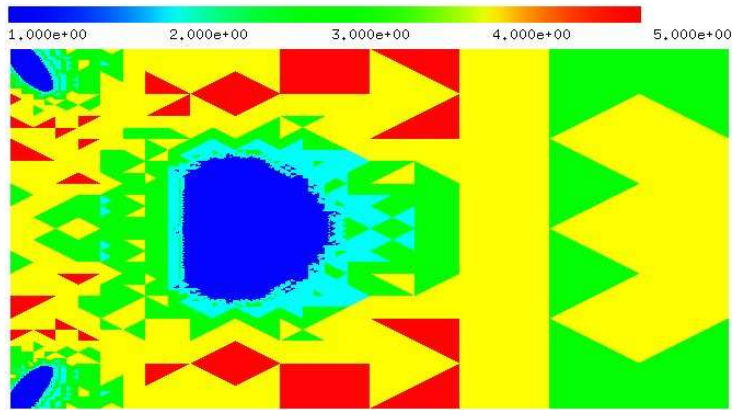
Figure 11: Polynomial order with Strategy 3 in Example 1.
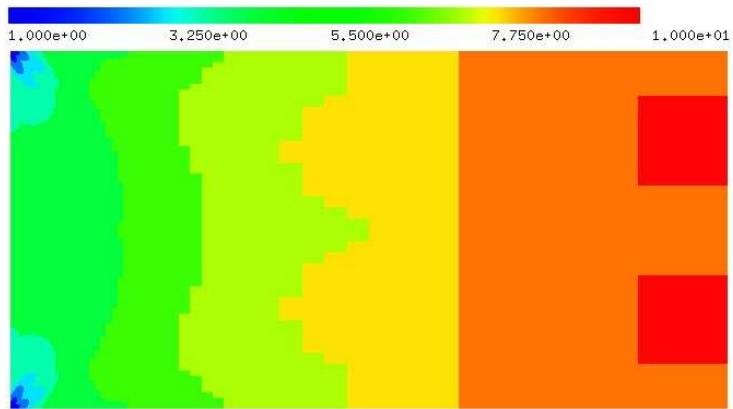
Figure 12: Polynomial order with Strategy 4 in Example 1.
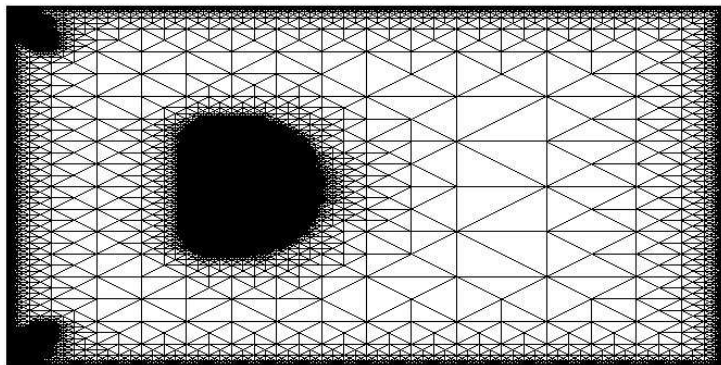
Figure 13: Adaptive mesh with Strategy 1 in Example 1.
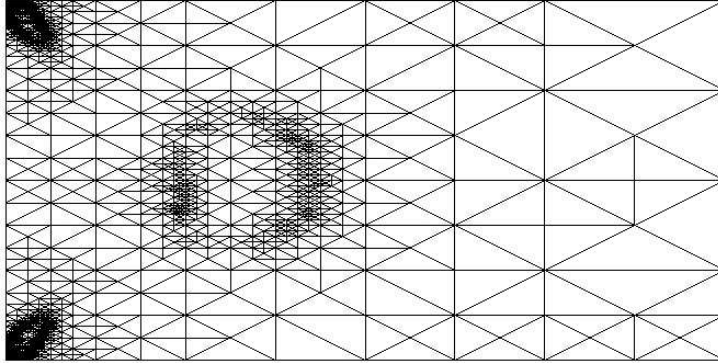
Figure 14: Adaptive mesh with Strategy 2 in Example 1.
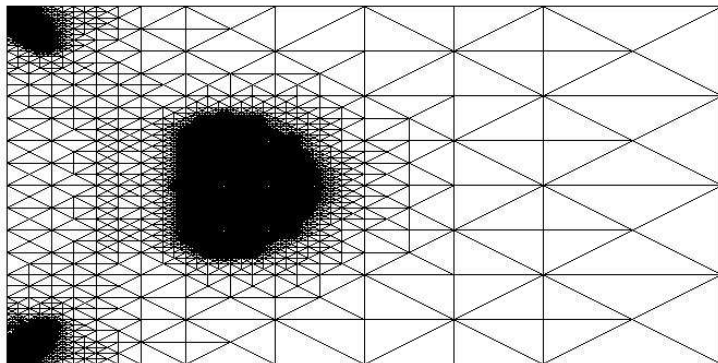
Figure 15: Adaptive mesh with Strategy 3 in Example 1.
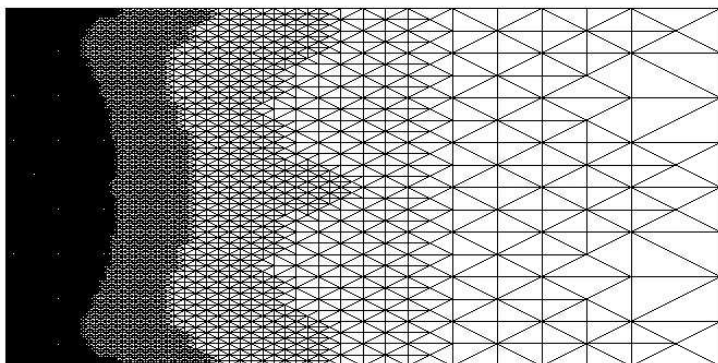

Figure 16: Adaptive mesh with Strategy 4 in Example 1.
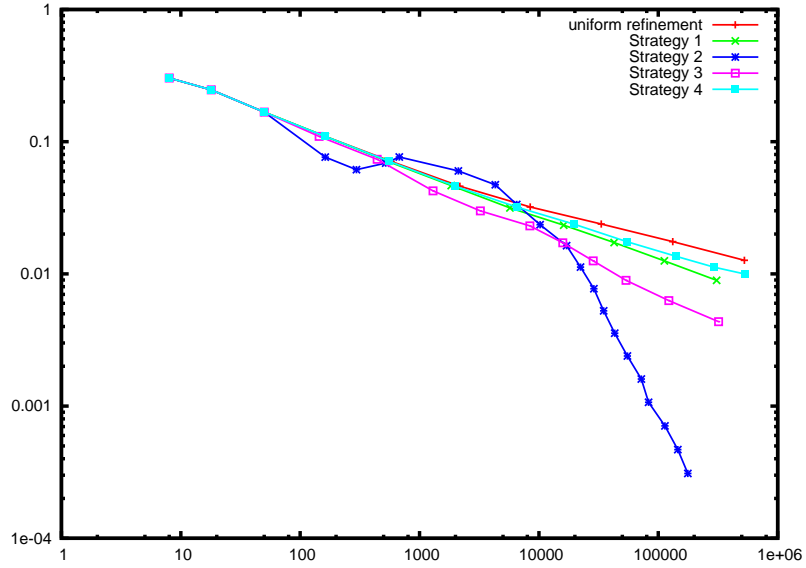
Figure 17: The global estimated error (45) versus degrees of freedom in Example 1.
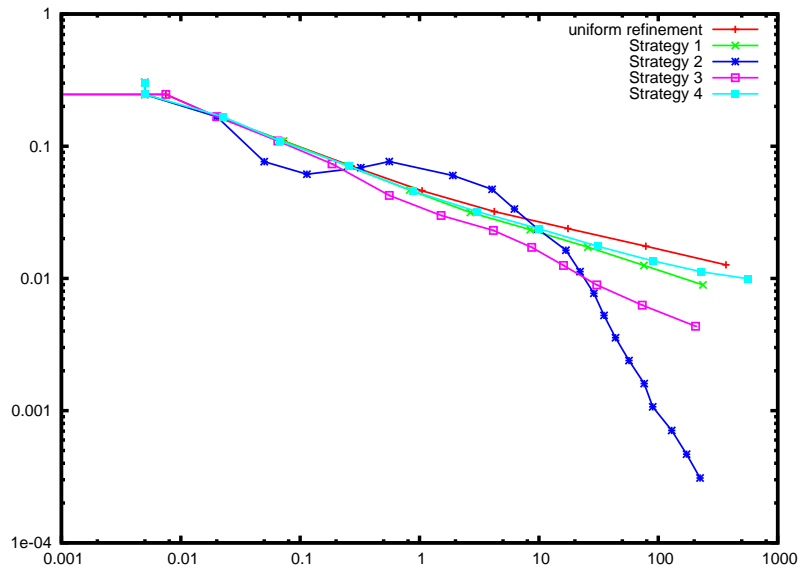

Figure 18: Here, the global estimated error (45) is plotted versus the time (in seconds) which was spent per Newton step in Example 1. One Newton step covers the assembling of the stiffness matrix and a sparse direct solver (PARDISO).

31

Example 2. A beam $\Omega = (0, 2) \times (-0.5, 0.5)$ is fixed on the boundary $\Gamma_D = \{(x, y) \in \partial\Omega \mid x \in (0, 0.5)\}$. On the boundary $\Gamma_N = \{(x, y) \in \partial\Omega \mid x \in (1.5, 2)\}$ a traction $g = (0.9, -\text{sign}(y) \, 0.1)$ is applied (see Figure 19). The material parameters are chosen as follows: Young's modulus $E = 1000$, Poisson ratio $\nu = 0.3$, yield stress $\sigma_y = 1$, and modulus of hardening $H = 10$. The graphical output after some steps of uniform refinement is as follows: The displacement is plotted in Figure 20, which also shows the deformation of the domain magnified by a factor 50. The yield function ϕ (8) is plotted in Figure 21. In Figure 22 the plastic zones (red) versus elastic zones (blue) are shown, whereas Figure 23 and Figure 24 report on the point-wise Frobenius-norm of the plastic strain. The estimated slope of the FE solution coefficients, as discussed in Algorithm 2, is plotted in Figure 25. We numerically tested uniform refinement (h-FEM) versus the hp-FE Strategies 1-4. Let be mentioned, that in all tests the super linear convergence of the Newton like method was observed. Figures 26-28 illustrate the polynomial order distribution after some steps of adaptive hp-refinement, whereas the resulting meshes are shown in Figures 30-32. The approximation error $\|u - u_{\text{FE}}\|_{H^1(\Omega)}$ is estimated by the elastic ZZ-error estimator (45). Figures 34 and 35 show the convergence results graphically.
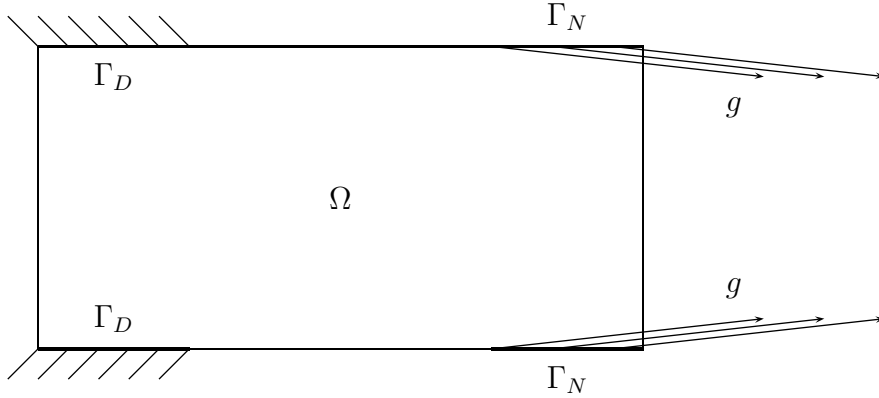
Figure 19: Geometry and problem description of Example 2.
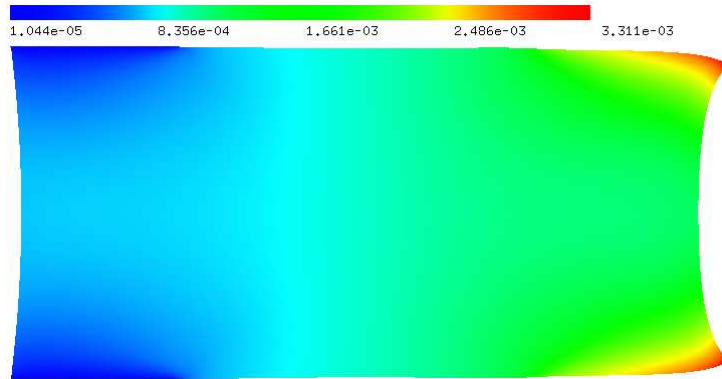
Figure 20: Displacement and deformed domain ($\times 50$) in Example 2.
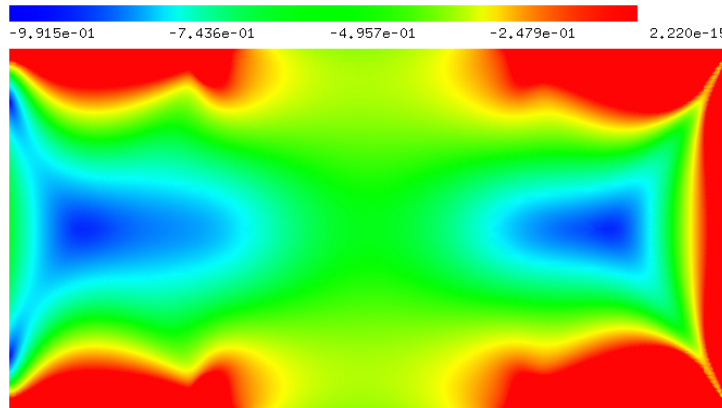
Figure 21: Yield function ϕ (8) in Example 2.

Figure 22: Plastic (red) and elastic (blue) zones in Example 2.

33
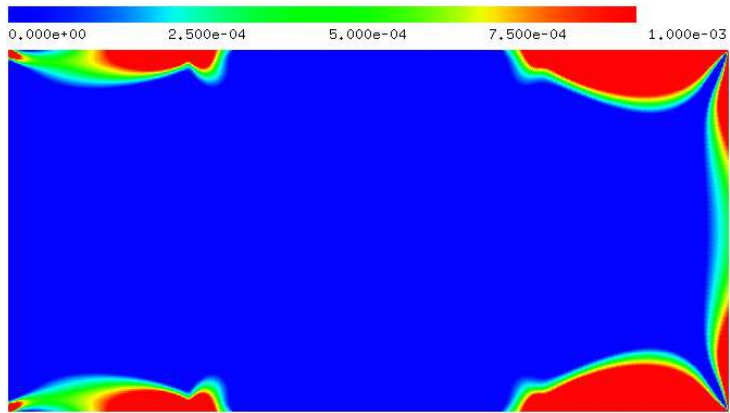
Figure 23: Frobenius norm of the plastic strain in Example 2.
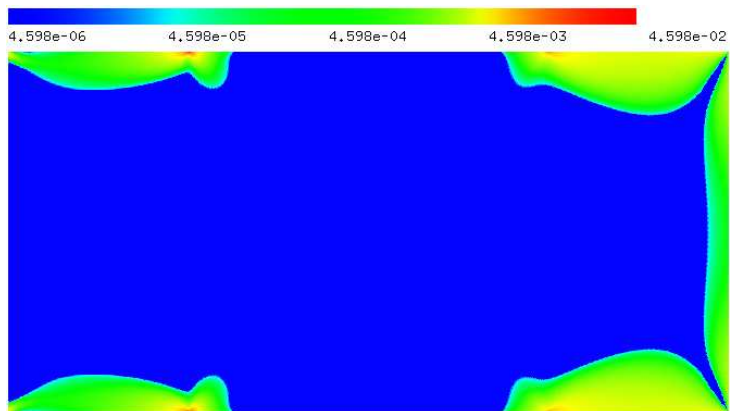
Figure 24: Logarithmic Frobenius norm of the plastic strain in Example 2.
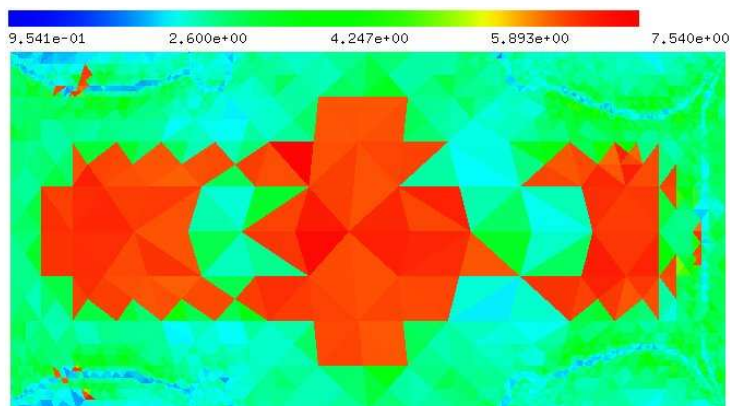
Figure 25: The estimated slope of coefficients (Algorithm 2) in Example 2.

34
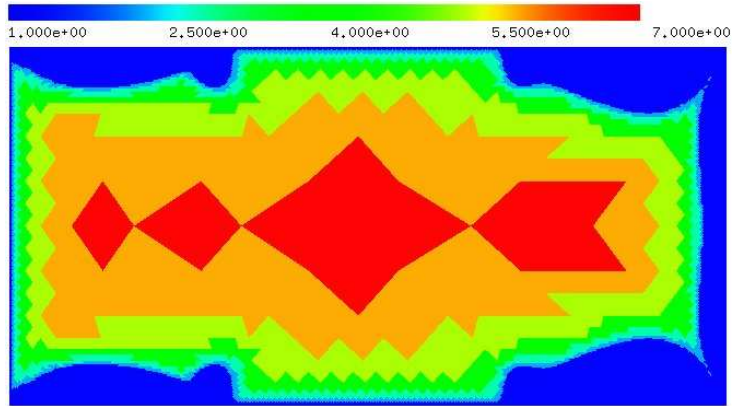
Figure 26: Polynomial order with Strategy 1 in Example 2.
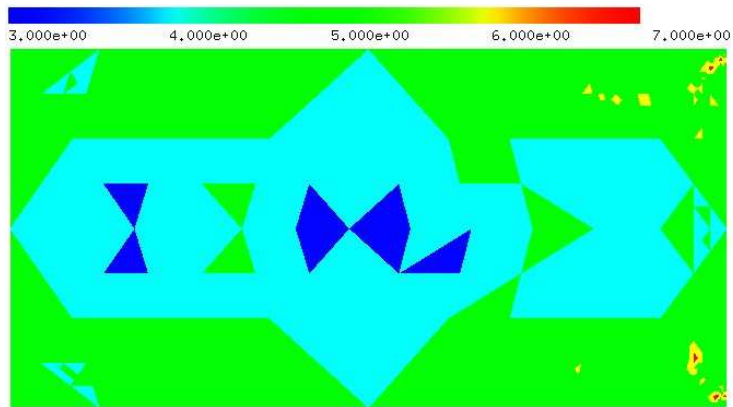
Figure 27: Polynomial order with Strategy 2 in Example 2.
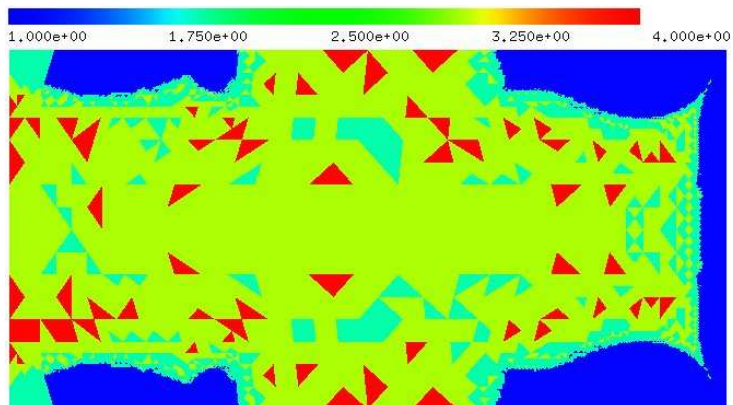
Figure 28: Polynomial order with Strategy 3 in Example 2.
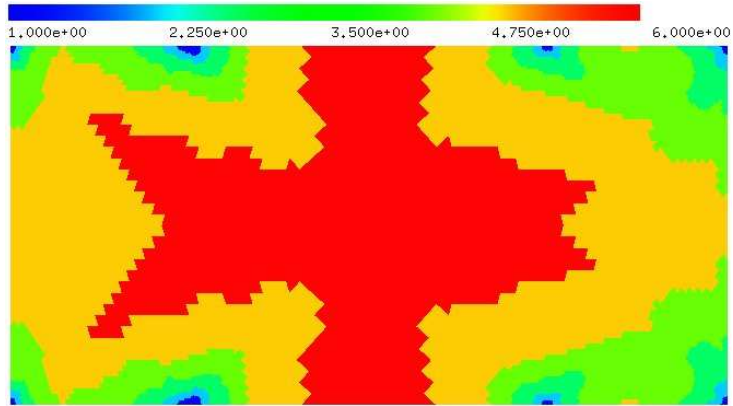
Figure 29: Polynomial order with Strategy 4 in Example 2.
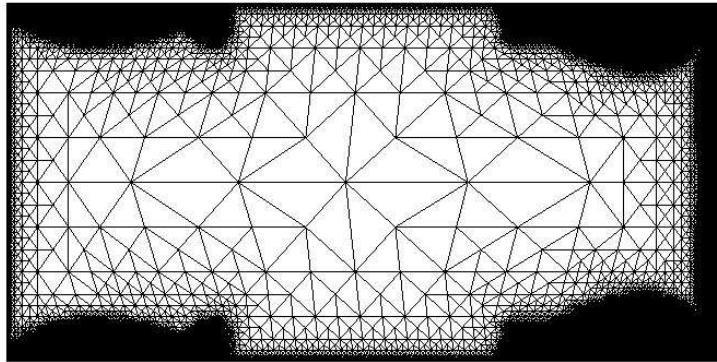
Figure 30: Adaptive mesh with Strategy 1 in Example 2.
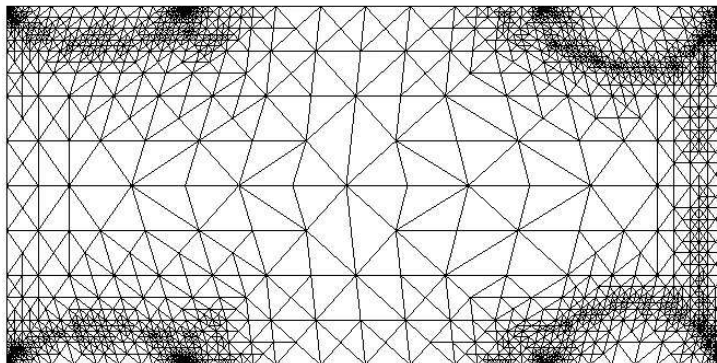
Figure 31: Adaptive mesh with Strategy 2 in Example 2.
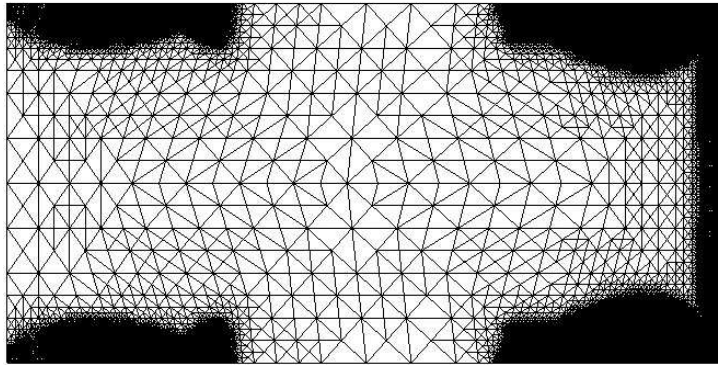
Figure 32: Adaptive mesh with Strategy 3 in Example 2.
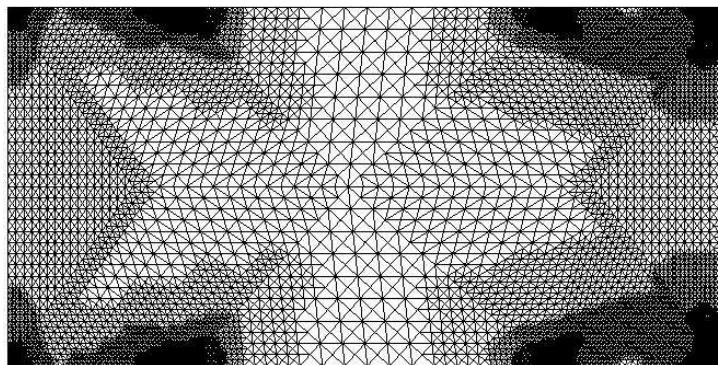
Figure 33: Adaptive mesh with Strategy 4 in Example 2.
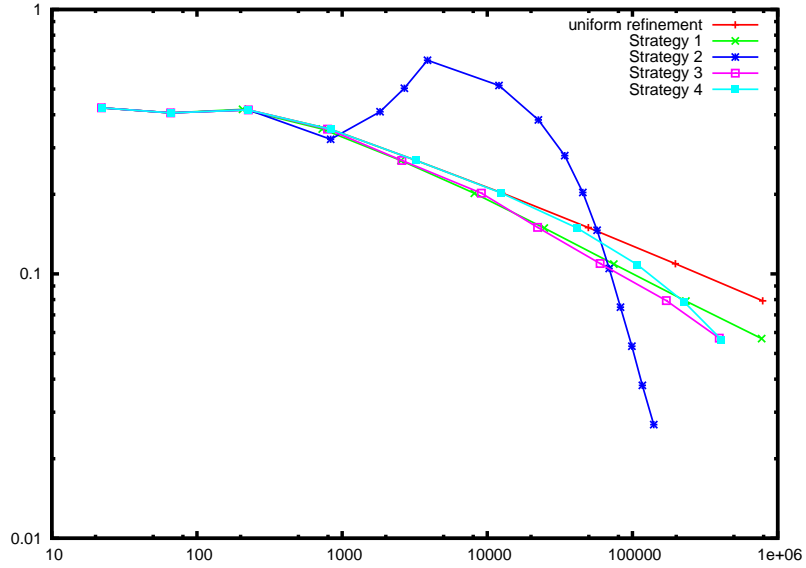
Figure 34: The global estimated error (45) versus degrees of freedom in Example 2.
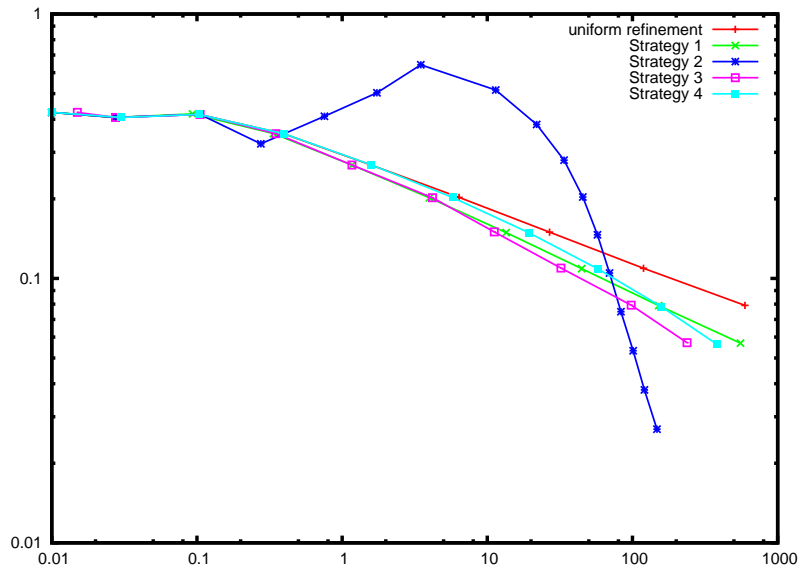
Figure 35: Here, the global estimated error (45) is plotted versus the time (in seconds) which was spent per Newton step in Example 2. One Newton step covers the assembling of the stiffness matrix and a sparse direct solver (PARDISO).

Example 3. A plate with a hole $\Omega = \{x \in [-10, 10]^2 : \|x\| \geq 1\}$ is torn on the top and bottom edges $\Gamma_N = \{(x, y) \in \partial\Omega \mid |y| = 10\}$ in normal direction with a traction of intensity $|g| = 450$. Due to the symmetry of the problem, only the top right quarter is considered in the numerical simulation (see Figure 36). Note, that gliding conditions are required on the cutting edges. The material parameters are chosen as follows: Young's modulus $E = 20690$, Poisson ratio $\nu = 0.29$, yield stress $\sigma_y = 450\sqrt{2/3}$, and modulus of hardening $H = 0.1$. The graphical output after some steps of uniform refinement is as follows: The displacement is plotted in Figure 37, which also shows the deformation of the domain magnified by a factor 100. The yield function ϕ (8) is plotted in Figure 38. In Figure 39 the plastic zones (red) versus elastic zones (blue) are shown, whereas Figure 40 and 41 report on the point-wise Frobenius-norm of the plastic strain. The estimated slope of the FE solution coefficients, as discussed in Algorithm 2, is plotted in Figure 42. We numerically tested uniform refinement (h-FEM) versus the hp-FE Strategies 1-4. Let be mentioned, that in all tests the super linear convergence of the Newton like method was observed. Figures 43-45 illustrate the polynomial order distribution after some steps of adaptive hp-refinement, whereas the resulting meshes are shown in Figures 47-49. The approximation error $\|u - u_{\mathrm{FE}}\|_{H^1(\Omega)}$ is estimated by the elastic ZZ-error estimator (45). Figures 51 and 52 show the convergence results graphically.
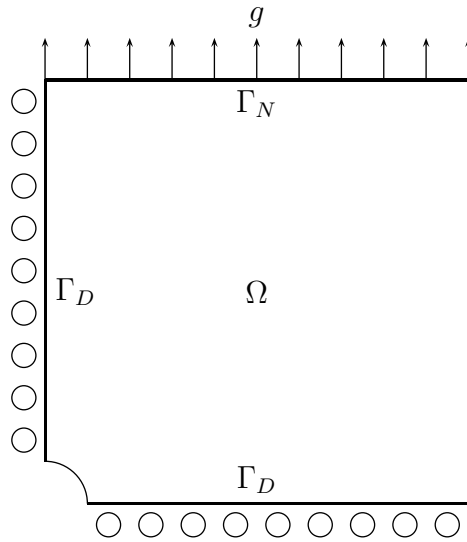
Figure 36: Geometry and problem description of Example 3.
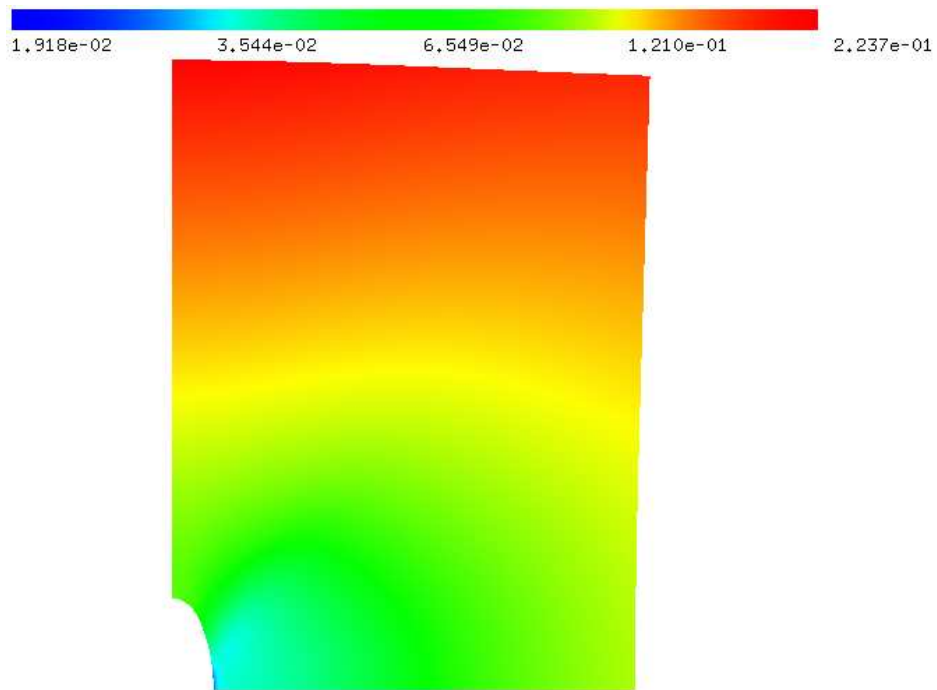
Figure 37: Displacement and deformed domain ($\times 100$) in Example 3.
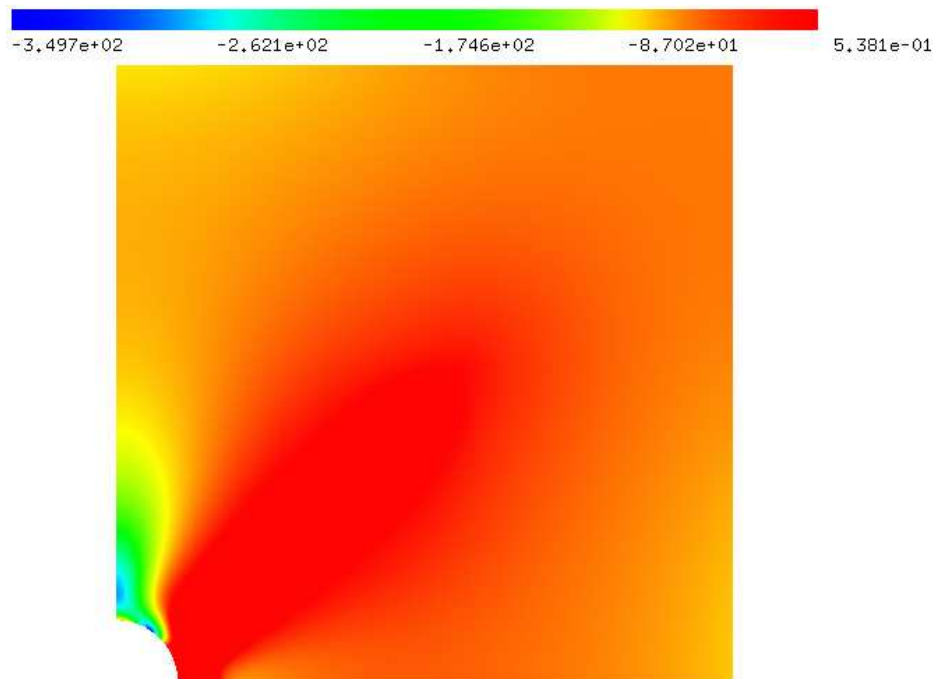
Figure 38: Yield function ϕ (8) in Example 3.
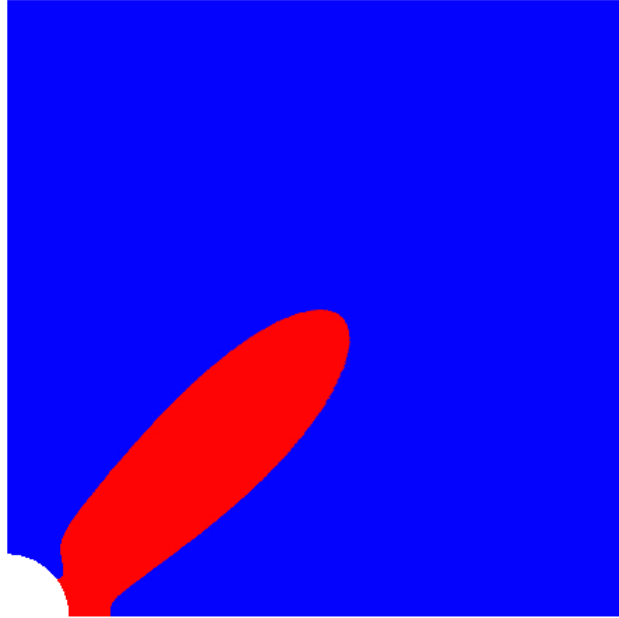
Figure 39: Plastic (red) and elastic (blue) zones in Example 3.
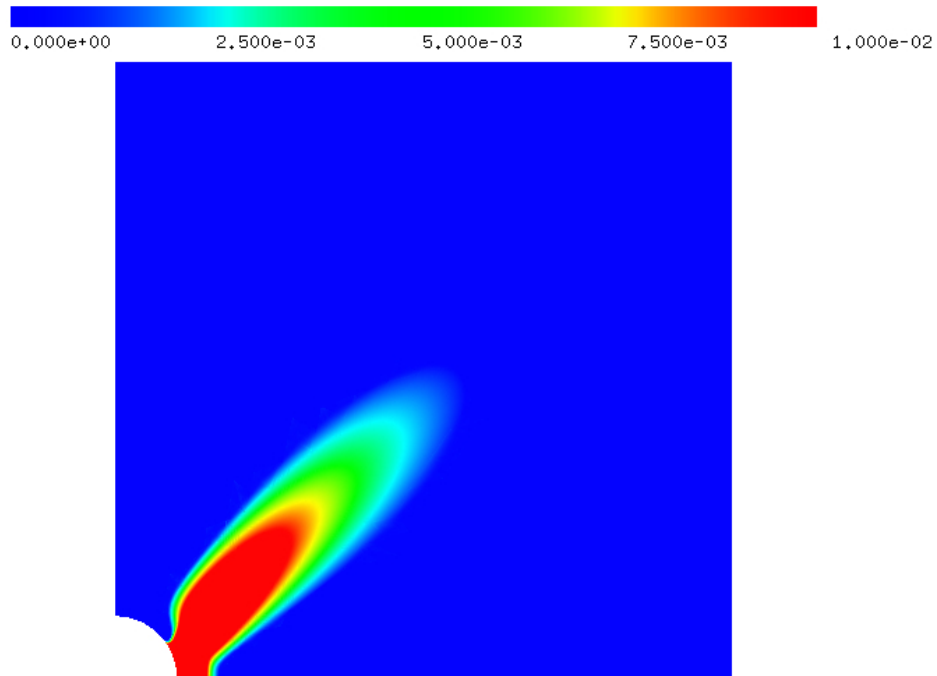

Figure 40: Frobenius norm of the plastic strain in Example 3.

41
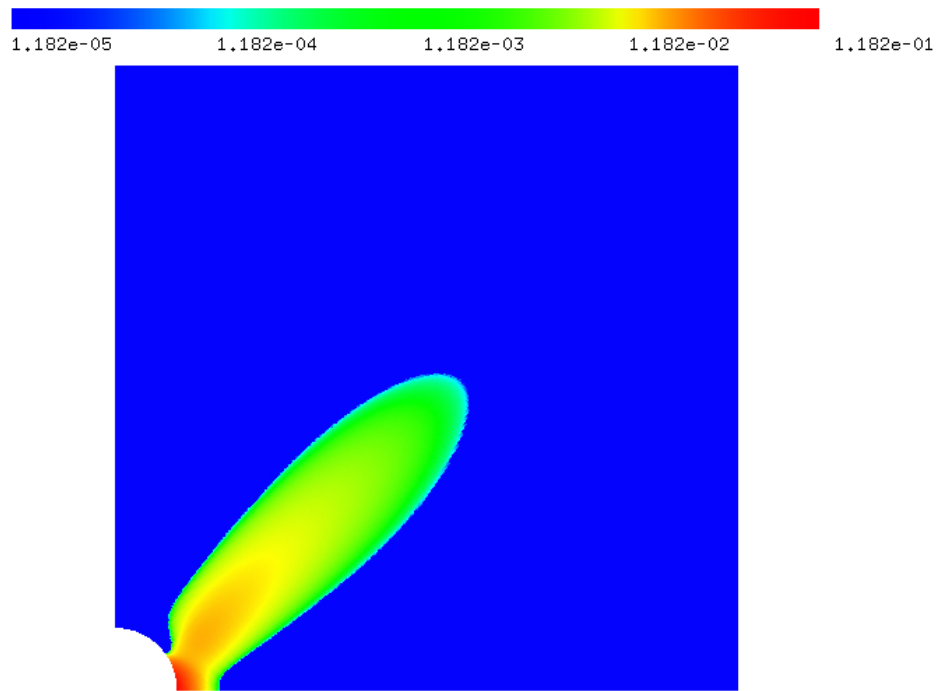
Figure 41: Logarithmic Frobenius norm of the plastic strain in Example 3.
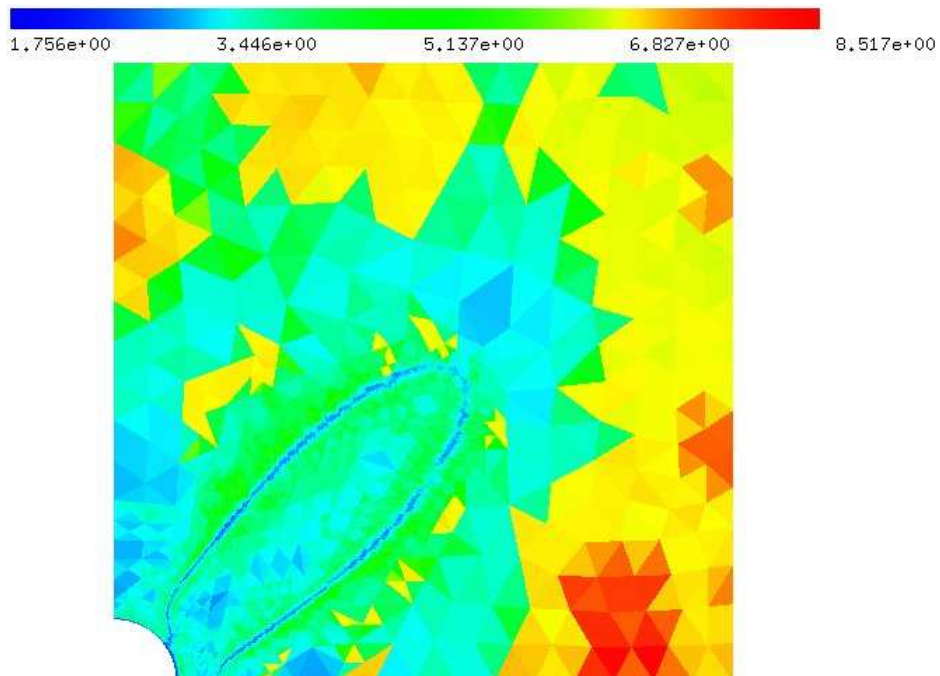
Figure 42: The estimated slope of coefficients (Algorithm 2) in Example 3.
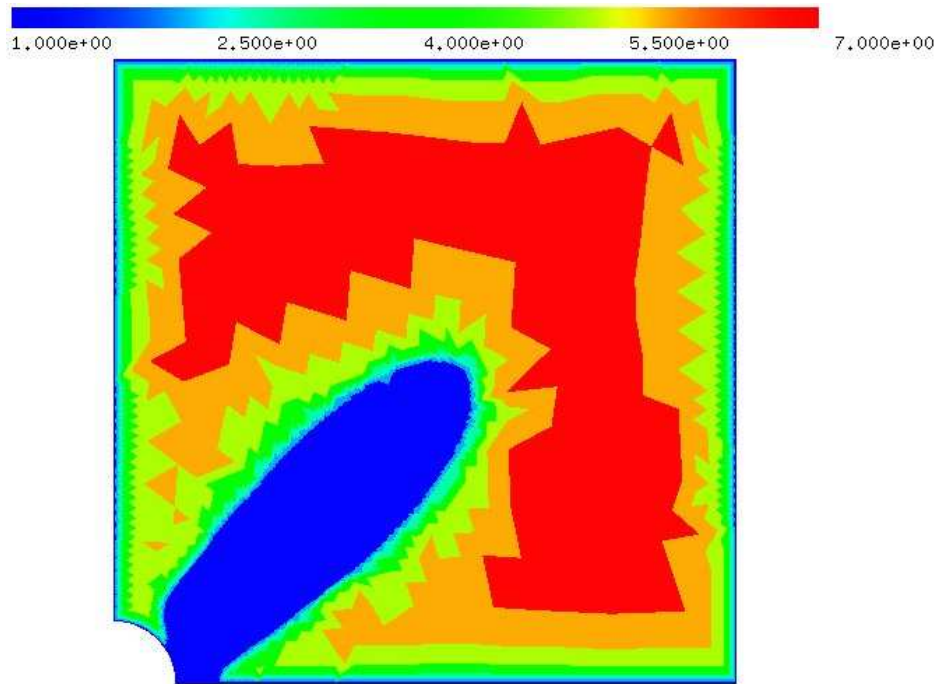
Figure 43: Polynomial order with Strategy 1 in Example 3.
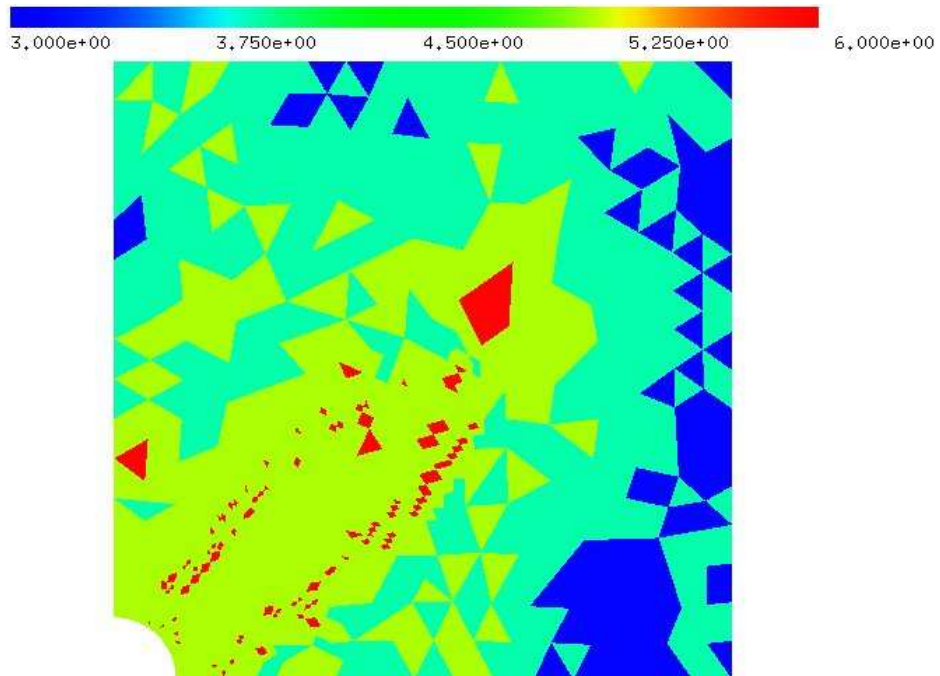


Figure 44: Polynomial order with Strategy 2 in Example 3.

43
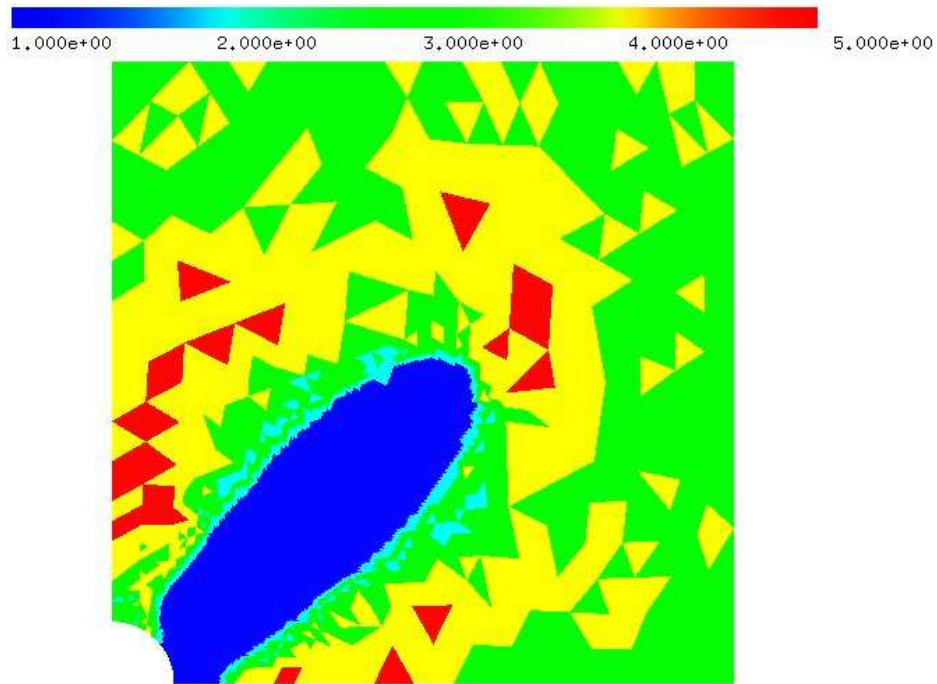
Figure 45: Polynomial order with Strategy 3 in Example 3.
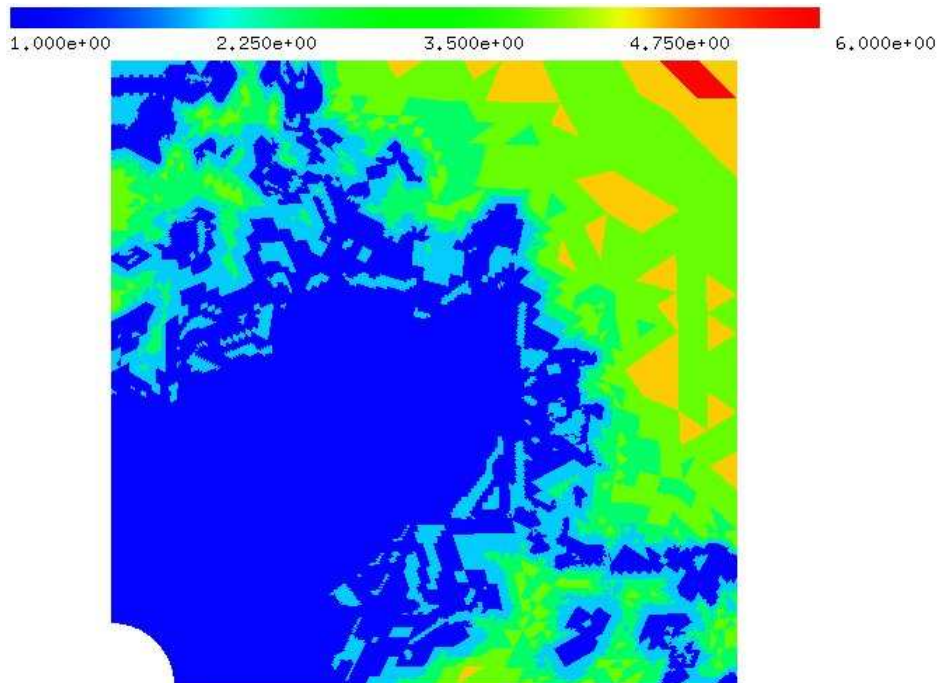
Figure 46: Polynomial order with Strategy 4 in Example 3.

44
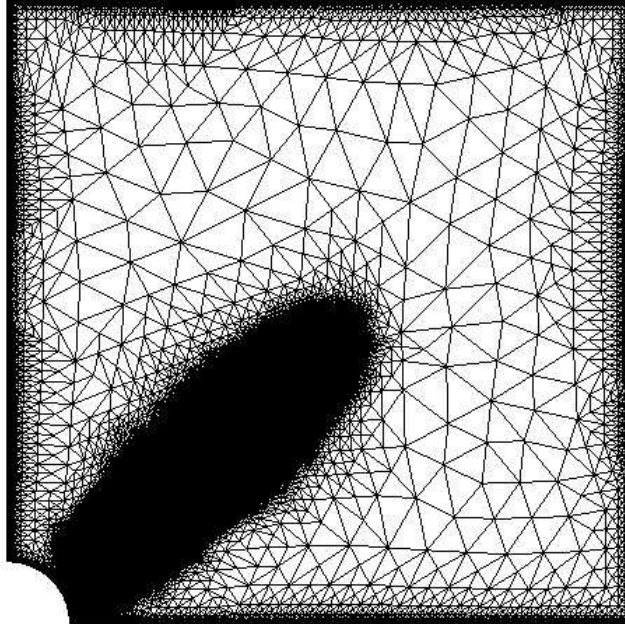
Figure 47: Adaptive mesh with Strategy 1 in Example 3.
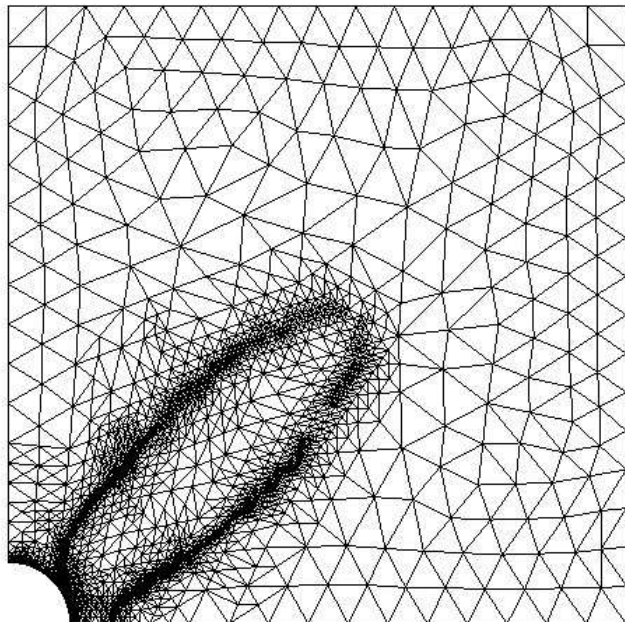
Figure 48: Adaptive mesh with Strategy 2 in Example 3.
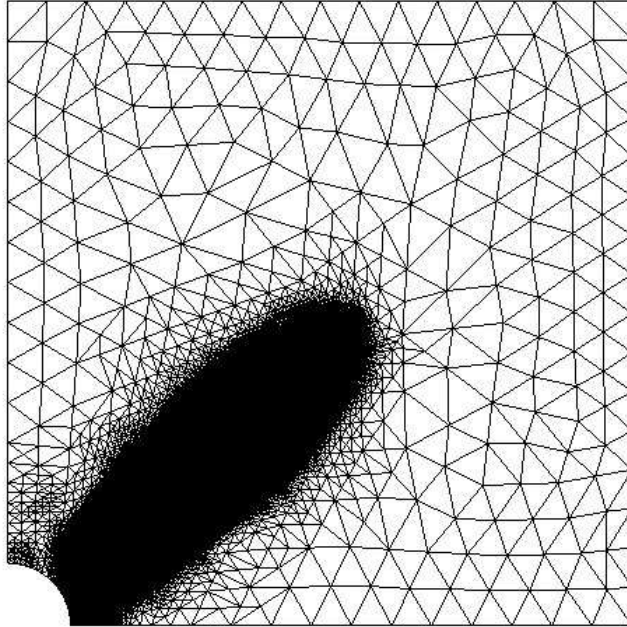
Figure 49: Adaptive mesh with Strategy 3 in Example 3.
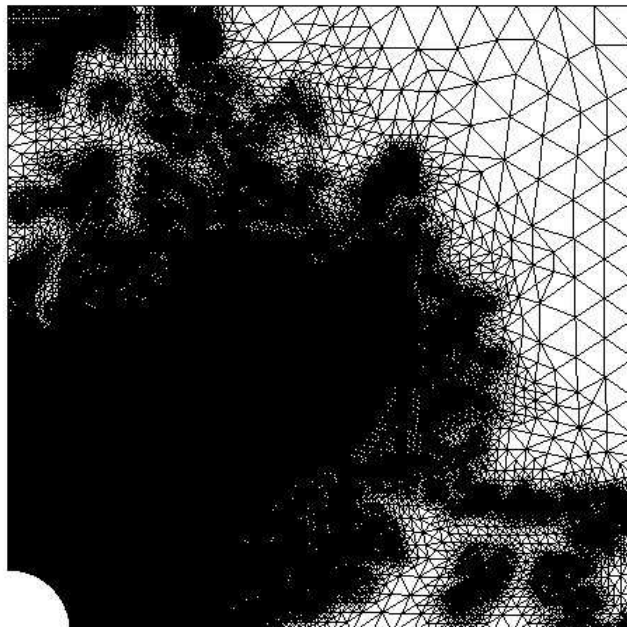
Figure 50: Adaptive mesh with Strategy 4 in Example 3.
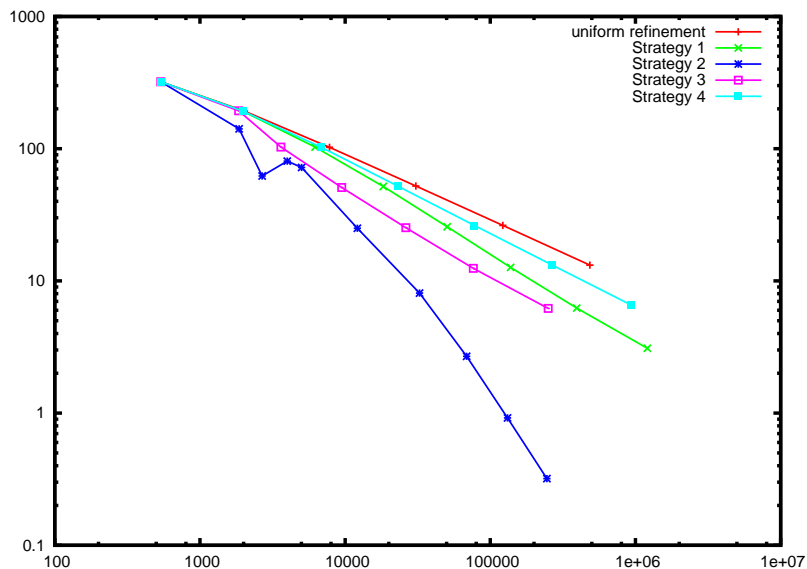
Figure 51: The global estimated error (45) versus degrees of freedom in Example 3.
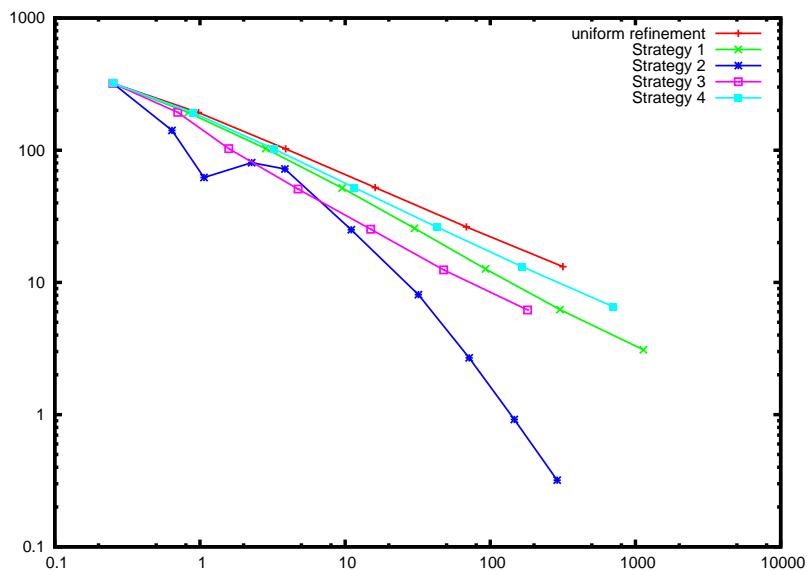

Figure 52: Here, the global estimated error (45) is plotted versus the time (in seconds) which was spent per Newton step in Example 3. One Newton step covers the assembling of the stiffness matrix and a sparse direct solver (PARDISO).

47

Conclusions

Let us finally discuss the convergence plots Figure 17, Figure 34, and Figure 51. Obviously, Strategy 2 works assymptotically best. However, in the first couple of refinements, the strategy seems to fail. This is due to the fact, that the polynomial degree has to be large enough, say greater than 4, for the method to work properly. Remember, the decision of whether to refine in h or in p is left to the least squares fit of a straight line through the pointcloud $(\ln|u_{pq}|, p + q)$, where u_{pq} denote the coefficients with respect to the expansion (44). So, the convergence of the FE-solution to the solution starts very late but fast in Strategy 2.

With Strategy 3, where we decide for h-refinement if an element was in the plastic zone, the convergence is not so fast assymptotically, but starts much earlier. This strategy seems to be best for real-time simulations.

Strategy 4 is not reliable. In many examples the author encountered a great loss of convergence rate at high levels of refinement (see Figure 17).

For Strategy 2 and Strategy 4 it is quite difficult to calibrate the parameters properly. Strategy 3 seemed to be less sensitive in this respect.

Despite the rather slow convergence rate in Strategy 1 (about twice as fast as when using uniform h-refinement), there is a big advantage: there are no parameters to adjust. This strategy works reliable in any case.

Acknowledgments

48

References

[1] M. AINSWORTH AND B. SENIOR, *Aspects of an adaptive hp-finite element method: adaptive strategy, conforming approximation and efficient solvers*, Comput. Methods Appl. Mech. Engrg., 150 (1997), pp. 65–87.

[2] H.-D. ALBER, *Materials with memory*, vol. 1682 of Lecture Notes in Mathematics, Springer-Verlag, Berlin, 1998. Initial-boundary value problems for constitutive equations with internal variables.

[3] J. ALBERTY, C. CARSTENSEN, S. A. FUNKEN, AND R. KLOSE, *Matlab implementation of the finite element method in elasticity*, Computing, 69 (2002), pp. 239–263.

[4] J. ALBERTY, C. CARSTENSEN, AND D. ZARRABI, *Adaptive numerical analysis in primal elastoplasticity with hardening*, Comput. Methods Appl. Mech. Engrg., 171 (1999), pp. 175–204.

[5] I. BABUSKA AND B. GUO, *The h-p version of the finite element method - Part 1: The basic approximation results*, Comput. Mech., 1 (1986), pp. 21–41.

[6] I. BABUŠKA AND M. SURI, *The h-p version of the finite element method with quasi-uniform meshes*, RAIRO Modél. Math. Anal. Numér., 21 (1987), pp. 199–238.

[7] ——, *The optimal convergence rate of the p-version of the finite element method*, SIAM J. Numer. Anal., 24 (1987), pp. 750–776.

[8] I. BABUŠKA, B. A. SZABO, AND I. N. KATZ, *The p-version of the finite element method*, SIAM J. Numer. Anal., 18 (1981), pp. 515–545.

[9] A. BECIROVIC, P. PAULE, V. PILLWEIN, A. RIESE, C. SCHNEIDER, AND J. SCHÖBERL, *Hypergeometric Summation Algorithms for High Order Finite Elements*, Computing, 78 (2006), pp. 235–249.

[10] A. BENSOUSSAN AND J. FREHSE, *Regularity results for nonlinear elliptic systems and applications*, vol. 151 of Applied Mathematical Sciences, Springer-Verlag, Berlin, 2002.

[11] S. BEUCHLER AND V. PILLWEIN, *Sparse shape functions for tetrahedral p-FEM using integrated Jacobi polynomials*, Computing, 80 (2007), pp. 345–375.

[12] ──, *Completions to sparse shape functions for triangular and tetrahedral p-FEM*, in Domain Decomposition Methods in Science and Engineering XVII, U. Langer, M. Discacciati, D. Keyes, O. Widlund, and W. Zulehner, eds., vol. 60 of Lecture Notes in Computational Science and Engineering, Heidelberg, 2008, Springer, pp. 435–442.

[13] R. BLAHETA, *Convergence of Newton-type methods in incremental return mapping analysis of elastoplastic problems*, Comput. Methods Appl. Mech. Engrg., 147 (1997), pp. 167–185.

[14] C. CARSTENSEN, *Domain decomposition for a non-smooth convex minimization problem and its application to plasticity*, Numer. Linear Algebra Appl., 4 (1997), pp. 177–190.

[15] ──, *Numerical analysis of the primal problem of elastoplasticity with hardening*, Numer. Math., 82 (1999), pp. 577–597.

[16] X. CHEN, Z. NASHED, AND L. QI, *Smoothing methods and semismooth methods for nondifferentiable operator equations*, SIAM Journal on Numerical Analysis, 38 (2000), pp. 1200–1216.

[17] P. G. CIARLET, *The finite element method for elliptic problems*, North-Holland Publishing Co., Amsterdam, 1978.

[18] L. DEMKOWICZ AND J. T. ODEN, *Application of hp-adaptive BE/FE methods to elastic scattering*, Comput. Methods Appl. Mech. Engrg., 133 (1996), pp. 287–317.

[19] L. DEMKOWICZ, J. T. ODEN, W. RACHOWICZ, AND O. HARDY, *Toward a universal h-p adaptive finite element strategy. I. Constrained approximation and data structure*, Comput. Methods Appl. Mech. Engrg., 77 (1989), pp. 79–112.

[20] L. DEMKOWICZ, W. RACHOWICZ, AND P. DEVLOO, *A fully automatic hp-adaptivity*, in Proceedings of the Fifth International Conference on Spectral and High Order Methods (ICOSAHOM-01) (Uppsala), vol. 17, 2002, pp. 117–142.

[21] L. DEMKOWICZ AND P. ŠOLÍN, *Goal-oriented hp-adaptivity for elliptic problems*, Comput. Methods Appl. Mech. Engrg., 193 (2004), pp. 449–468.

[22] G. DUVAUT AND J. L. LIONS, *Inequalities in mechanics and physics*, Springer-Verlag, Berlin, 1976. Translated from the French by C. W. John, Grundlehren der Mathematischen Wissenschaften, 219.

[23] T. Eibner and J. M. Melenk, *An adaptive strategy for hp-FEM based on testing for analyticity*, Comput. Mech., 39 (2007), pp. 575–595.

[24] I. Ekeland and R. Témam, *Convex analysis and variational problems*, vol. 28 of Classics in Applied Mathematics, Society for Industrial and Applied Mathematics (SIAM), Philadelphia, PA, english ed., 1999. Translated from the French.

[25] R. Glowinski, J.-L. Lions, and R. Trémolières, *Numerical analysis of variational inequalities*, vol. 8 of Studies in Mathematics and its Applications, North-Holland Publishing Co., Amsterdam, 1981. Translated from the French.

[26] P. G. Gruber and J. Valdman, *Solution of one-time-step problems in elastoplasticity by a slant Newton method*, SIAM J. Sci. Comput., 31 (2009), pp. 1558–1580.

[27] W. Han and B. D. Reddy, *Plasticity: mathematical theory and numerical analysis*, vol. 9 of Interdisciplinary Applied Mathematics, Springer-Verlag, New York, 1999. Mathematical theory and numerical analysis.

[28] N. Heuer, M. E. Mellado, and E. P. Stephan, *hp-adaptive two-level methods for boundary integral equations on curves*, Computing, 67 (2001), pp. 305–334.

[29] M. Hintermüller, K. Ito, and K. Kunisch, *The primal-dual active set strategy as a semismooth Newton method*, SIAM J. Optim., 13 (2002), pp. 865–888.

[30] P. Houston and E. Süli, *A note on the design of hp-adaptive finite element methods for elliptic partial differential equations*, Comput. Methods Appl. Mech. Engrg., 194 (2005), pp. 229–243.

[31] C. Johnson, *Existence theorems for plasticity problems*, J. Math. Pures Appl. (9), 55 (1976), pp. 431–444.

[32] G. E. Karniadakis and S. J. Sherwin, *Spectral/hp element methods for CFD*, Oxford University Press, New York, 1999.

[33] B. N. Khoromskij and J. M. Melenk, *Boundary concentrated finite element methods*, SIAM J. Numer. Anal., 41 (2003), pp. 1–36.

[34] J. Kienesberger, *Efficient Solution Algorithms for Elastoplastic Problems*, PhD thesis, Johannes-Kepler-Universität Linz, 2006.

[35] J. KIENESBERGER, U. LANGER, AND J. VALDMAN, *On a robust multigrid-preconditioned solver for incremental plasticity problems*, in Proceedings of IMET 2004 - Iterative Methods, Preconditioning & Numerical PDEs, 2004, pp. 84–87.

[36] D. KNEES AND P. NEFF, *Regularity up to the boundary for nonlinear elliptic systems arising in time-incremental infinitesimal elasto-plasticity*, SIAM J. Math. Anal., 40 (2008), pp. 21–43.

[37] V. G. KORNEEV AND U. LANGER, *Approximate solution of plastic flow theory problems*, vol. 69 of Teubner-Texte zur Mathematik [Teubner Texts in Mathematics], BSB B. G. Teubner Verlagsgesellschaft, Leipzig, 1984.

[38] C. MAVRIPLIS, *Adaptive mesh strategies for the spectral element method*, Comput. Methods Appl. Mech. Engrg., 116 (1994), pp. 77–86.

[39] J. M. MELENK, *hp-finite element methods for singular perturbations*, vol. 1796 of Lecture Notes in Mathematics, Springer, Berlin, 2002.

[40] J. J. MOREAU, *Proximité et dualité dans un espace hilbertien*, Bull. Soc. Math. France, 93 (1965), pp. 273–299.

[41] J. T. ODEN, L. DEMKOWICZ, W. RACHOWICZ, AND T. A. WESTERMANN, *Toward a universal h-p adaptive finite element strategy. II. A posteriori error estimation*, Comput. Methods Appl. Mech. Engrg., 77 (1989), pp. 113–180.

[42] J. T. ODEN, W. WU, AND M. AINSWORTH, *Three-step h-p adaptive strategy for the incompressible Navier-Stokes equations*, in Modeling, mesh generation, and adaptive numerical methods for partial differential equations (Minneapolis, MN, 1993), vol. 75 of IMA Vol. Math. Appl., Springer, New York, 1995, pp. 347–366.

[43] W. RACHOWICZ, J. T. ODEN, AND L. DEMKOWICZ, *Toward a universal h-p adaptive finite element strategy. III. Design of h-p meshes*, Comput. Methods Appl. Mech. Engrg., 77 (1989), pp. 181–212.

[44] J. SCHÖBERL, *NETGEN/NGSolve - Finite Element solver software package.* URL: http://www.hpfem.jku.at/netgen/.

[45] C. SCHWAB, *p- and hp- finite element methods: theory and applications in solid and fluid mechanics*, Oxford University Press, New York, 1998.

[46] J. C. Simo and T. J. R. Hughes, *Computational inelasticity*, vol. 7 of Interdisciplinary Applied Mathematics, Springer-Verlag, New York, 1998.

[47] E. Stein, *Error-controlled Adaptive Finite Elements in Solid Mechanics*, Wiley, Chichester, 2003.

[48] C. Wieners, *Multigrid methods for finite elements and the application to solid mechanics. Theorie und Numerik der Prandtl-Reuß Plastizität*, 2000. Habilitationsschrift, Universität Heidelberg, Germany.

[49] ———, *Nonlinear solution methods for infinitesimal perfect plasticity*, Tech. Rep. 11, IWRMM, Universität Karlsruhe, 2006.

Technical Reports of the Doctoral Program
"Computational Mathematics"

2010

2010-01   S. Radu, J. Sellers: *Parity Results for Broken k-diamond Partitions and (2k+1)-cores* March 2010. Eds.: P. Paule, V. Pillwein

2010-02   P.G. Gruber: *Adaptive Strategies for High Order FEM in Elastoplasticity* March 2010. Eds.: U. Langer, V. Pillwein

2009

2009-01   S. Takacs, W. Zulehner: *Multigrid Methods for Elliptic Optimal Control Problems with Neumann Boundary Control* October 2009. Eds.: U. Langer, J. Schicho

2009-02   P. Paule, S. Radu: *A Proof of Sellers' Conjecture* October 2009. Eds.: V. Pillwein, F. Winkler

2009-03   K. Kohl, F. Stan: *An Algorithmic Approach to the Mellin Transform Method* November 2009. Eds.: P. Paule, V. Pillwein

2009-04   L.X.Chau Ngo: *Rational general solutions of first order non-autonomous parametric ODEs* November 2009. Eds.: F. Winkler, P. Paule

2009-05   L.X.Chau Ngo: *A criterion for existence of rational general solutions of planar systems of ODEs* November 2009. Eds.: F. Winkler, P. Paule

2009-06   M. Bartoň, B. Jüttler, W. Wang: *Construction of Rational Curves with Rational Rotation-Minimizing Frames via MöbiusTransformations* November 2009. Eds.: J. Schicho, W. Zulehner

2009-07   M. Aigner, C. Heinrich, B. Jüttler, E. Pilgerstorfer, B. Simeon, A.V. Vuong: *Swept Volume Parameterization for Isogeometric Analysis* November 2009. Eds.: J. Schicho, W. Zulehner

2009-08   S. Béla, B. Jüttler: *Fat arcs for implicitly defined curves* November 2009. Eds.: J. Schicho, W. Zulehner

2009-09   M. Aigner, B. Jüttler: *Distance Regression by Gauss–Newton–type Methods and Iteratively Re–weighted Least–Squares* December 2009. Eds.: J. Schicho, W. Zulehner

2009-10   P. Paule, S. Radu: *Infinite Families of Strange Partition Congruences for Broken 2-diamonds* December 2009. Eds.: J. Schicho, V. Pillwein

2009-11   C. Pechstein: *Shape-explicit constants for some boundary integral operators* December 2009. Eds.: U. Langer, V. Pillwein

2009-12   P. Gruber, J. Kienesberger, U. Langer, J. Schöberl, J. Valdman: *Fast solvers and a posteriori error estimates in elastoplasticity* December 2009. Eds.: B. Jüttler, P. Paule

2009-13   P.G. Gruber, D. Knees, S. Nesenenko, M. Thomas: *Analytical and Numerical Aspects of Time-Dependent Models with Internal Variables* December 2009. Eds.: U. Langer, V. Pillwein

Doctoral Program

"Computational Mathematics"